LA-UR-13-22466

Title: LANL Deliverable to the Big Sky Carbon Sequestration Partnership: Preliminary CO2-PENS model

Author(s):   Stauffer, Philip H.
Dai, Zhenxue
Lu, Zhiming
Middleton, Richard S.
Jacobs, John F.
Carey, James W.

Intended for: Report

Los Alamos
NATIONAL LABORATORY
—— EST. 1943 ——

LANL Deliverable to the Big Sky Carbon Sequestration Partnership

Preliminary CO$_2$-PENS model

Subtask 4.8– Performance/Risk Assessment

March 31, 2013

P.H. Stauffer, Z. Dai, Z. Lu, R. Middleton, J. Jacobs, B. Carey

Executive Summary

The preliminary sub-surface risk assessment for the Kevin Dome includes limited risk factors based on available data. The analysis is presented in five sections. In the first section, we review the Features, Events, and Processes (FEPs) applicable to the CO_2-PENS model based on a larger set of FEPs developed by Schlumberger. The CO_2-PENS applicable will be expanded in future work as site-specific data become available. The FEPs addressed in this report include

1) Injectivity and the number of injection wells needed for project success;
2) CO_2 plume extent that will feed future calculations of wellbore, fault, and caprock leakage risks;
3) Performance of production wells related to the projects ability to deliver enough CO_2 to meet project goals; and
4) Caprock leakage due to uncertainty in the caprock permeability.

The second section of the report (Section 2) describes the CO_2-PENS risk assessment model of injectivity assuming a homogeneous reservoir and is designed to capture the impact of large uncertainties in injectivity on the number of injection wells needed and the radius of the injected plume that are due to very limited site-specific data. Results suggest that if the plume is able to access permeable thickness on the order of 20 m with a mean permeability of 30 milidarcys (md), plume radius is likely to be on the order of 1.7 to 3 km, while the number of wells needed ranges from 1 to 4 (mean of 2.28). Thinner high porosity zones with a mean permeability of 100 md and average thickness of 3 m lead to plumes radii of 3.5 to 5 km with from 2 to 7 wells required for injection (mean of 4). Because the project is required to have a single injection well, we will need to intersect permeability equivalent to approximately one 20 m section of average permeability combined with two thin higher permeability zones to achieve success. High resolution 3-D seismic density inversions would be extremely useful to have before the injection site is located.

Section 3 describes initial results for a heterogeneous reservoir that involves creating multiple realizations of porosity and permeability heterogeneity in the injection and production intervals. Estimates of heterogeneity based on site-specific core data will be used to reduce uncertainty in project risk associated with both injectivity and plume growth. The workflow will allow rapid turnaround when site-specific data become available.

Section 4 present an analysis of likely pressure drops associated with production wells. These results provide our initial description of project risk and performance related to well productivity. Because the mobility of nearly pure CO_2 in the production zone is high relative to the effective mobility in the injection zone, required permeability in the production zone can be lower than that required in the injection zone to meet project goals.

Finally, in Section 5, we describe our path forward and include discussion of how the work-to-date will guide the continued development of the CO_2-PENS subsurface risk model as we add complexity and increasing amounts of site-specific data with the ultimate goal of reducing project risk.

1. Features, Events, and Processes (FEPs) applicable to the CO2-PENS model

The following is a working outline of FEPs that will be considered for inclusion in the subsurface risk/system modeling using CO_2-PENS and related software. The deliverable related to this document states

> "In the preliminary risk assessment for the Kevin Dome site, BSCSP will identify the factors to be included using the CO_2-PENS model and determine how the process level information will be addressed."

CO_2-PENS and associated software such as SimCCS and FEHM combine elements of subsurface risk with larger system level risk associated with CO_2 sources, transport, distribution, and brine treatment. Subsurface risks and uncertainties that are part of the CO_2-PENS framework include:

a) leakage of both brine and CO_2 from the storage reservoir through faults, caprocks, and wells;
b) contamination of groundwater or overlying resources through leakage of both brine and CO_2;
c) reservoir storage capacity; and
d) reservoir injectivity and related well drilling costs.

Additionally, LANL is in the process of implementing:

e) new algorithms in CO_2-PENS to estimate seismicity risks.

Through coupling of SimCCS to CO_2-PENS, we are also able to address

f) regional evaluation of source (CO_2 emissions) to sink (EOR or sequestration sites) couplings and feedbacks, desalination/brine treatment costs, pipeline distribution, and well placement

The Schlumberger draft risk assessment (Oct 2011) is used as a guide to provide suggestions for processes to include in the CO_2-PENS/System level risk modeling. In the attached Tables 11-13 (Appendix A), 138 FEPs have been ranked, and the FEPs of most concern are shown for three different metrics. The first metric is overall risk (probability x severity), the second metric is based solely on severity, and the third metric highlights 'Black Swan' FEPs that have low probability but relatively high impact.

In these tables, processes that CO_2-PENS and associated software could be useful for include the following:

a) CO_2 Delivery System: Source Composition ranked 3rd in table 11
    i. Could impact CO_2-PENS leakage if CO_2 contains trace H_2S for example.
    ii. Related to SimCCS because of pipelines concerns.

iii. Could impact injectivity through geochemical feedback on near injector permeabilities. This is not currently in CO_2-PENS but could be explored in collaboration with LBNL.

b) CO_2 injectate effects: Groundwater contamination: Public perception, ranked 5th in table 11,
   i. Relates to CO_2-PENS leakage and groundwater plume calculations

c) Placement and Performance of Production Wells, 7th in table 11
   i. Relates to SimCCS calculations (source sink pipelines etc).

d) Reservoir injectivity, ranked 8th in table 11; 10th in table 12
   i. Relates to CO_2-PENS Injectivity calculations. Could collaborate with LBNL and use their reservoir simulation results as input to some set of CO_2-PENS calculations.

e) Seismicity (project-induced earthquakes) 14th in table 11
   i. LANL is working to develop CO_2-PENS capabilities in this area. We would likely run coupled flow/stress calcs to inform CO_2-PENS reduced order models.

f) Pressure: Reservoir overpressuring 22nd in table 12 and last on table 13
   i. Relates to CO_2-PENS Storage-Injectivity-Leakage calculations. We currently address overpressure by calculating brine production needed to reduce pressure to acceptable values. Coupled to this analysis are the costs for brine treatment.

g) Caprock or confining formation: Primary 24th in table 12
   i. Relates to CO_2-PENS Leakage calcs. For example, at the Rock Springs Uplift, we ran 42 reservoir simulation realizations to explore caprock leakage due to uncertain permeability distributions.

h) Contamination of groundwater 26th in table 12
   i. Relates to CO_2-PENS leakage and groundwater plume calcs

i) Seal failure 29th in table 12 AND 2nd on Table 13.
   i. Relates to CO_2-PENS leakage and groundwater plume calculations through both caprock leakage (porous flow) and fault flow through both known and unknown faults. Fault leakage is under development and could be beta tested on Big Sky.

j) Fractures and faults open pathway
   i. Relates to CO_2-PENS leakage via fault flow through both known and unknown faults. Fault leakage is under development and could be beta tested on Big Sky.

k) Pressure effects on caprock 9th table 13
   i. Relates to CO_2-PENS leakage and groundwater plume calcs through both caprock leakage (porous flow) and fault flow through both known and unknown faults. Fault leakage is under development and could be beta tested on Big Sky.

For the current deliverable, we address four of these possible FEPs (a-d). Caprock leakage (a) is presented as part of heterogeneous 3-D reservoir simulations in Section 3. Initial work on CO_2 injectate effects (b) is presented in Section 2 through estimates of uncertainty in the CO_2 plume radius, especially in relationship to the locations of known wells that penetrate the Duperow. Production performance (c) is explored in Section 4 through both analytical and 2-D radial numerical simulations of pressure drawdown. Reservoir injectivity (d) is modeled using both CO_2-PENS and 2-D radial reservoir simulations in Section 2.

2. Preliminary CO₂-PENS model

In this section we present results from simulations of injectivity and plume radius using the CO_2-PENS simulator (Stauffer et al., 2009, 2010; Viswanathan et al., 2009; Keating et al., 2011; Middleton et al., 2012). The injection site for the Big Sky project is located at a depth of approximately 1100 m below ground surface.
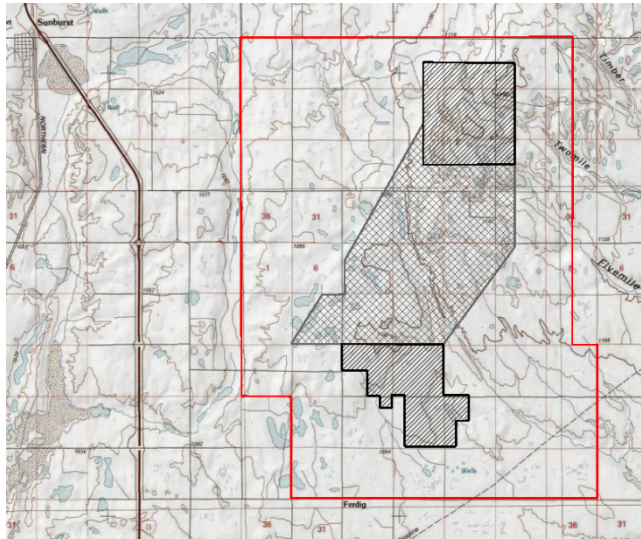

Figure 2-1 Site location. The hatched square in the top right is the planned injection area while the irregular hatched region toward the bottom is the planned production area. The town of Sunburst, MT is to the upper left and each small square is 1.67 km (1 mile) on a side.

As shown in Figure 2-2, at this depth, maximum injection pressure could be from 16.5 MPa (65% lithostatic) to 20 MPa (80% lithostatic). Because the state of stress in the subsurface is unknown, the maximum injection pressure for the simulations presented is taken as the low end of this range (16.5 MPa).
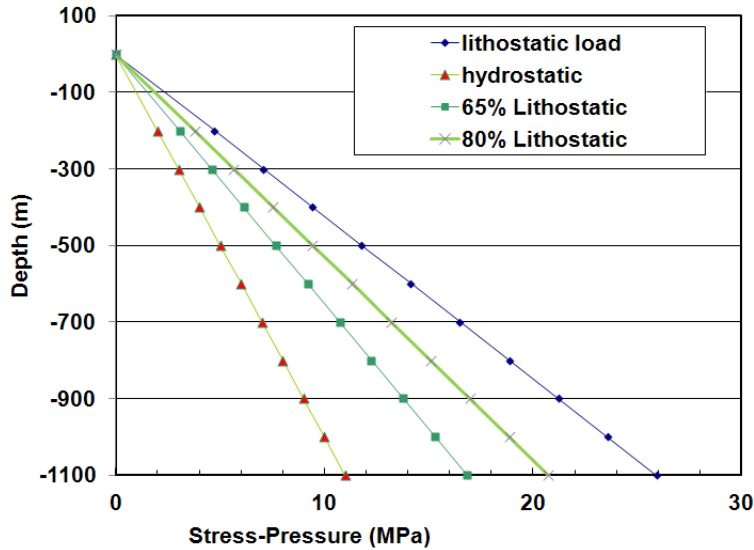
Figure 2-2 Stress and pressure versus depth

No site-specific core or log data exist for the planned injection area and we use data provided by Dave Bowen for a well within 15km of the site that penetrates the targeted Middle Duperow injection horizon (pers. com.). Figure 2-3 shows that well log data through the injection interval has porosity greater than 5% with a maximum of near 20%. Permeability for the lower porosity sections of the injection horizon are thought to average near 25 md (milidarcys = 1e-15 m^2), while for the higher porosity bands the mean may be closer to 100 md (Dave Bowen and Quanlin Zhou, pers. com.)
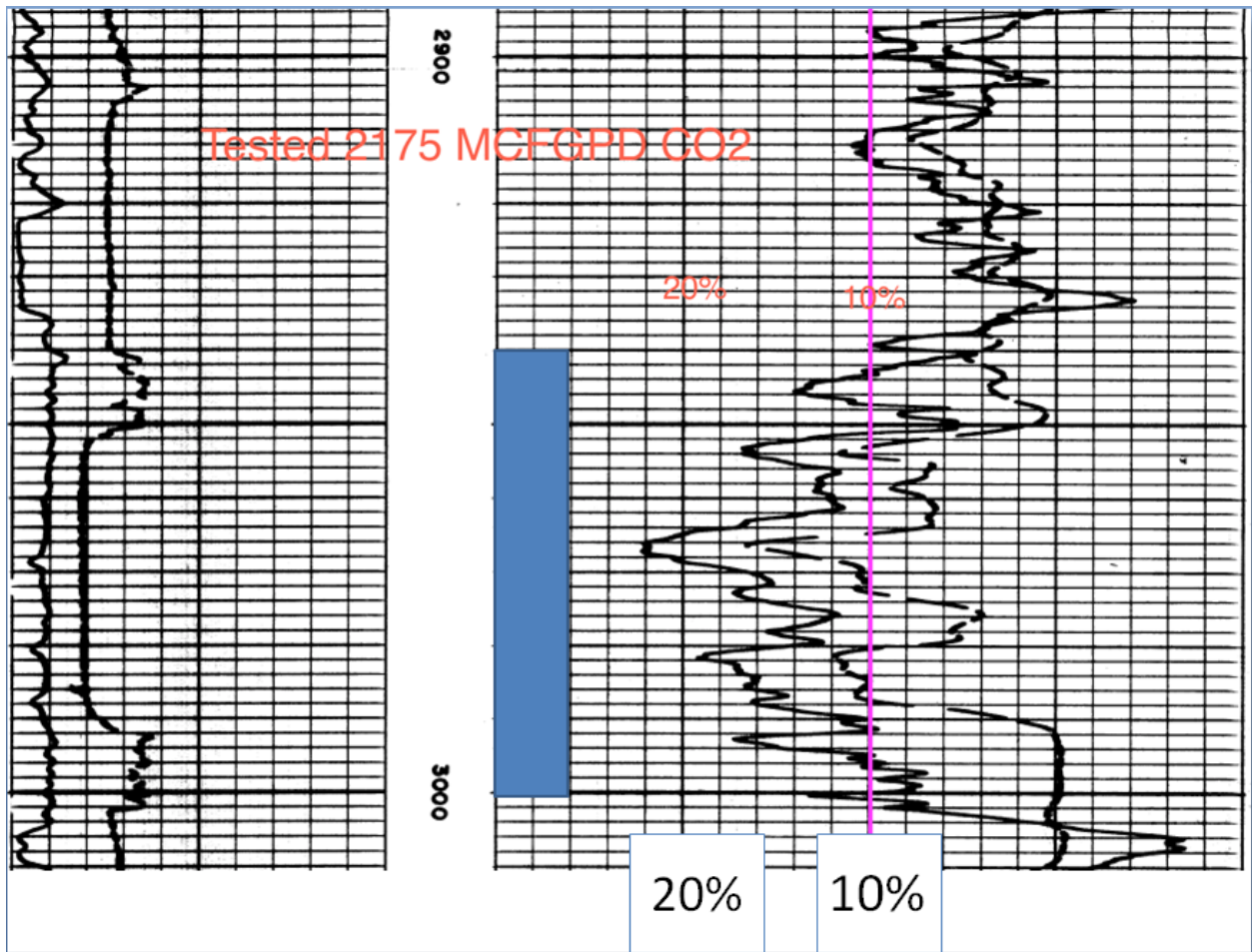
Figure 2-3 Well log data for a CO_2 producing well in the Kevin Dome area. The permeable section is approximately 16 m thick (blue bar), with high and low porosity estimates based on neutron and gamma logs. Note that this well tested at rate of 45kt of CO_2 per year during a short flow test.

Using these data, the CO_2-PENS model was run for 100 realizations for two cases. The first case (Case 1 PENS) is a permeable section having a mean thickness of 20 m, mean porosity of 0.1, and mean permeability of 25 md. The second case explores the ability of higher permeability (100 md mean) thin layers (3 m mean) to accept CO_2 injection (Case 2 PENS). Figures 2-4 and 2-5 show the distributions used to span a wide range of uncertainty in each of these parameters for both cases.
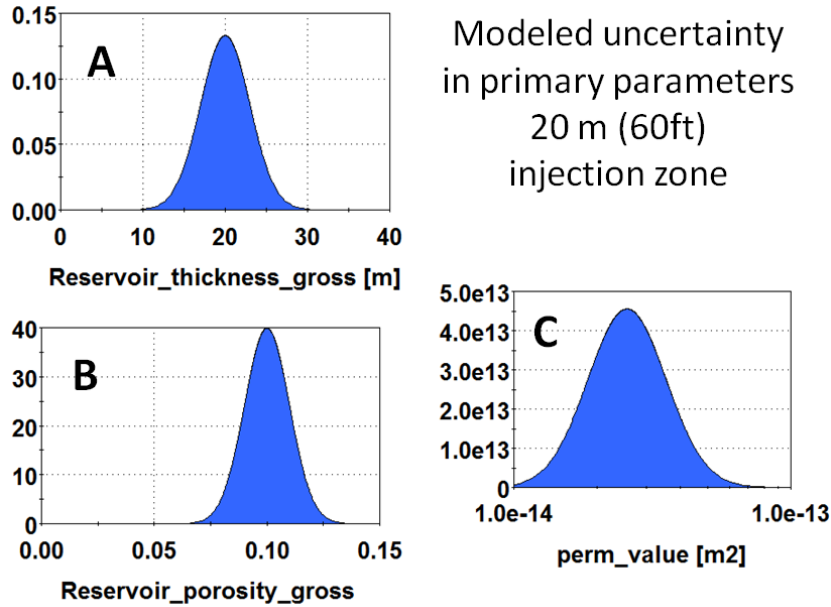
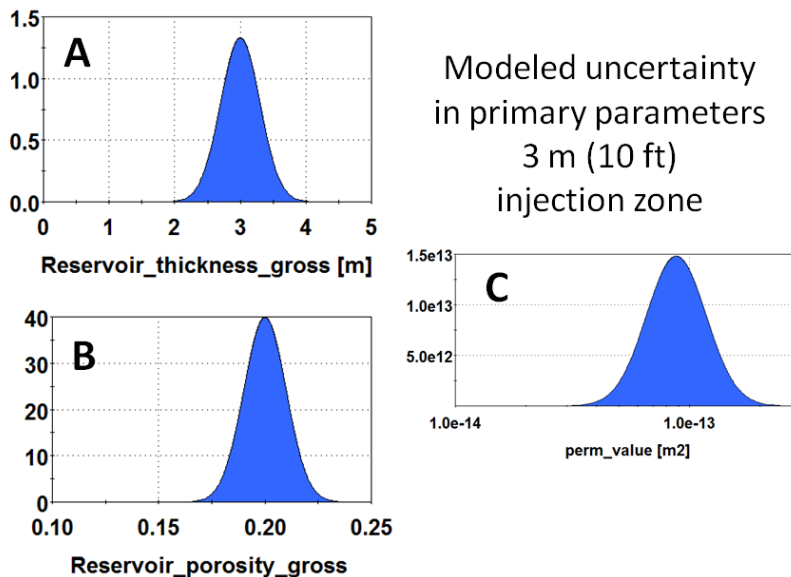Figure 2-4 Parameter uncertainty used in Case 1.

Figure 2-5 Parameter uncertainty used in Case 2.

During the analysis, we checked individual FEHM runs versus the CO_2-PENS results and determined that for the thicker units, CO_2-PENS was within a 10% of FEHM for all spot checks. However, the reduced order model (ROM) used in CO_2-PENS was not trained properly for the thin units. To address this problem in the current report we have increased the CO_2-PENS injectivity values for the thin units by a factor of 1.5. In the longer term, this analysis will allow us to create a more robust ROM that includes model training in thinner units. The ROM used in these simulations predicts injectivity assuming a linear relative permeability curve with zero residual saturation for both CO_2 and water, and a far-field boundary fixed at hydrostatic pressure.
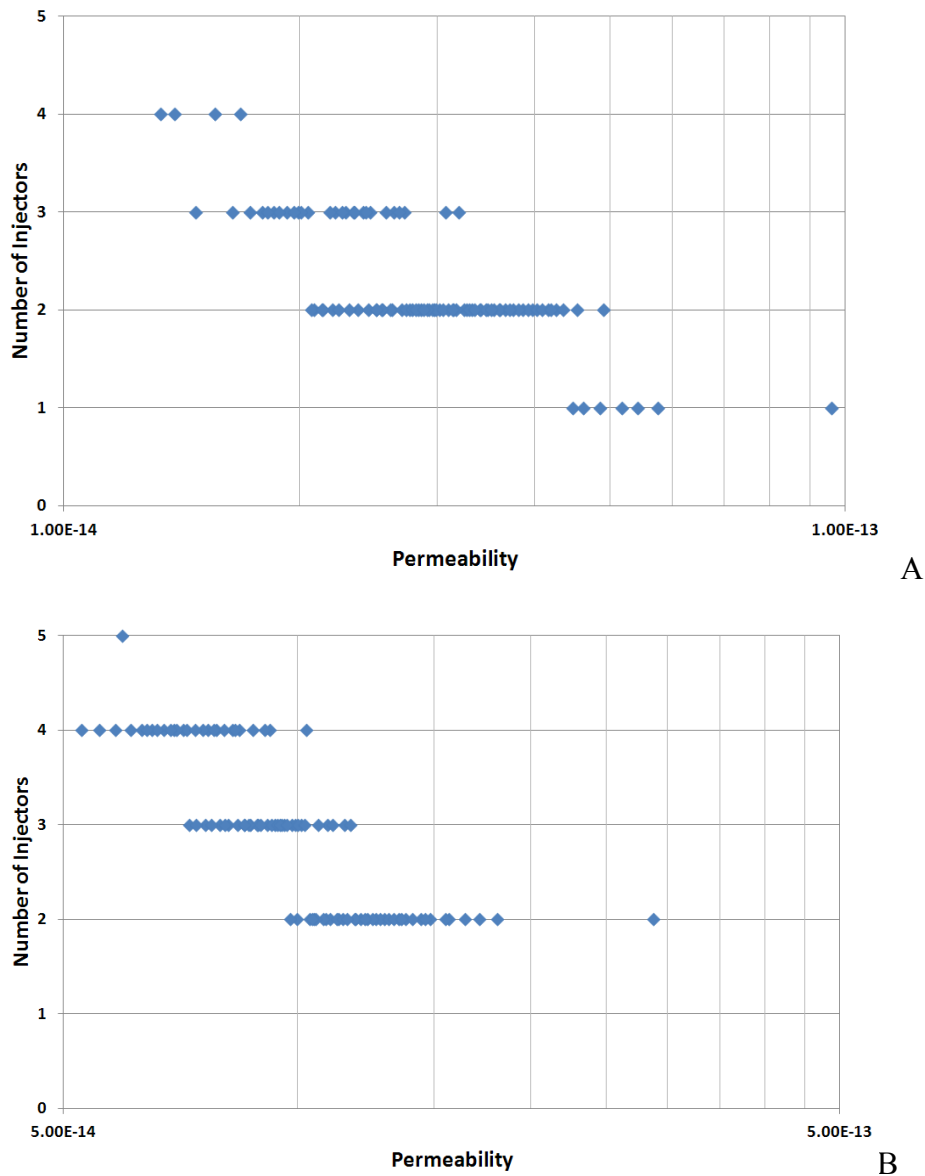
Figure 2-6 Number of injectors needed for A) Case 1 (thick) and B) Case 2 (thin) as a function of permeability.

Injectivity results for the two cases are shown in figure 2-6. The mean number of injection wells for the thick case (Case 1) is 2.28, with some cases needing as many as four wells. Only 7% of the runs in Case 1 needed a single injector. Results for Case 2 (thin) show are shifted to higher numbers of injectors needed for a given realization with a mean of 2.94. In order to satisfy the project target of 1 injector well, the current results imply that we need a combination of both an average thick unit with two average thin high permeability horizons. Because porosity in the

Middle Duperow can change from one location to another over the span of 100s of meters, locating an injection well a priori carries significant risk that 1 injection well could be insufficient if lower than expected porosity is encountered. It is clear that using 3-D seismic density interpretation to locate the projects single injection well should be of the highest priority given the high consequence of drilling into a lower porosity section of the Middle Duperow. Alternatively, having a backup plan in place to drill horizontally to access increased permeability could allow more latitude in choosing the drilling location of the injection well without additional geologic data.

Plume radii for the 100 realizations of Case 1 (thick) and Case 2 (thin) are shown in Figure 2-7. These results are generated using the analytical sharp interface solution of Nordbotten et al. (2005) assuming a residual water saturations of 0.5 and 0.0. Project risk associated with placement of monitoring wells should take into consideration these calculations. For example, at zero residual saturation, a monitoring well placed at 2 km from the injection well would be predicted to have an 89% chance of intersecting the plume, while a well placed at 2.5 km would have a success rate of only 16%. This analysis should be repeated as more data become available to guide final location of monitoring wells.
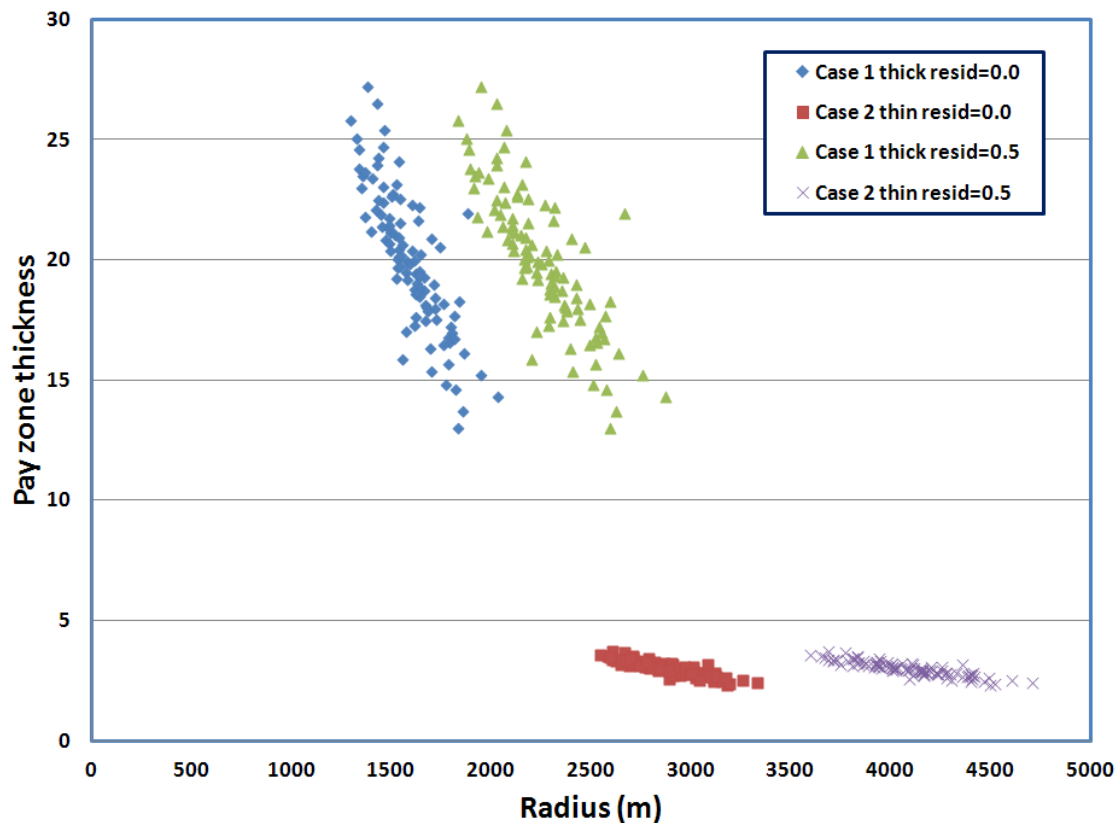

Figure 2-7 Range of calculated CO_2 plume radii for Cases 1 and 2.

3. <u>Heterogeneous reservoir modeling of the Middle Duperow (Zhenxue Dai)</u>

In this section, we illustrate the workflow that will be used to develop a CO_2-PENS risk assessment model that includes heterogeneity in the injection zone.

Kevin Dome is a large geologic feature that covers roughly 700 square miles in Toole County, Montana. The stratigraphy of the Kevin Dome is shown in Figure 3-1. The target reservoir is the middle Duperow Formation, with a thickness between 20 m and 58 m (Eggie et al., 2012). The production zone is located at a depth of around 1000 m and the injection at around 1100 m. The permeability values in the middle Duperow are between 2.5×10^{-15} and 2.5×10^{-12} m^2 and a porosity between 5 and 25 %. The caprock, consisting of variable formations (e.g. upper Duperow formation (~91 m thickness), Nisku formation (15-23 m thickness), and Potlatch formation (~ 53 m thickness), has a mean total thickness around 160 m and a much lower permeability (between 2.5×10^{-19} and 2.5×10^{-15} m^2) and porosity (1-5%). The lower Duperow lies below the target reservoir and is used as the "bedrock" in the model with a thickness around 90 m, in which the permeability and porosity distributions are similar to the upper caprock. Table 3-1 lists the parameter uncertainties for the injection reservoir and caprocks.

The reservoir simulator FEHM (Zyvoloski et al., 2011) was used to simulate the CO_2 flow and transport in the Kevin Dome field. In this analysis, we start with a 2-dimensional radial model and then go to a 3-dimensional model. A cross section of the model is presented in Figure 3-2. In order to define an appropriate numerical grid, a few grid test cases were conducted and presented in the Appendix B.
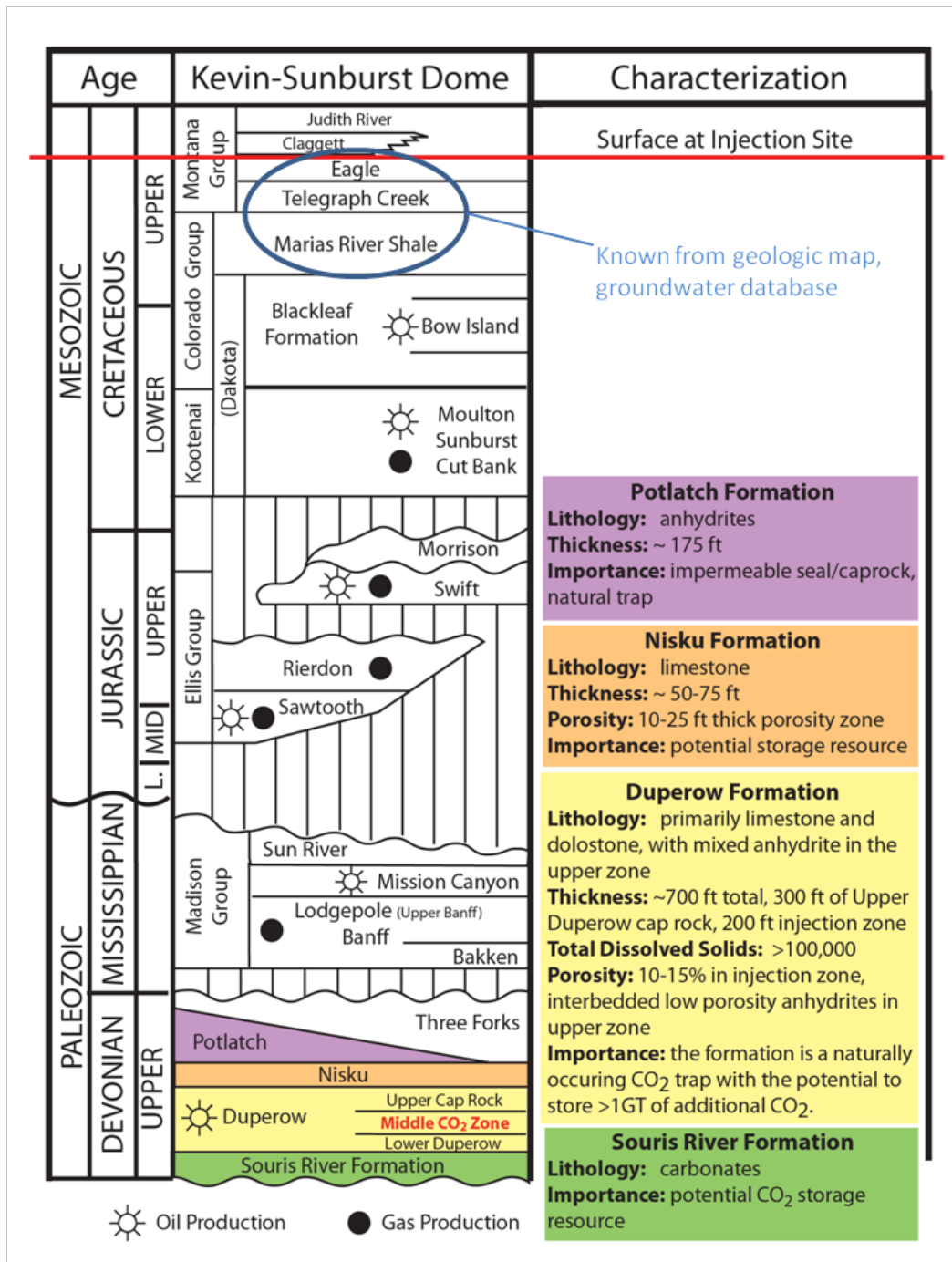
Figure 3-1: The stratigraphy of the Kevin Dome site

Table 3-1: Parameter uncertainty for the Kevin Dome site

Parameter		Min.	Max.
Reservoir (middle Duperow)	Reservoir thickness (m)	20.0	58.0
	Reservoir permeability (log m^2)	-15.6	-11.6
	Anisotropy factor	1.0	50
	Reservoir porosity	5%	25%
	Permeability variance(σ^2)	0.1	0.5
	Permeability scale (λ, km)	0.1	1.0
Caprock	Caprock porosity	constant	0.08
	Caprock perm (log m^2)	constant	-16
Injection	Scaled CO_2 injection rate	0	1.0
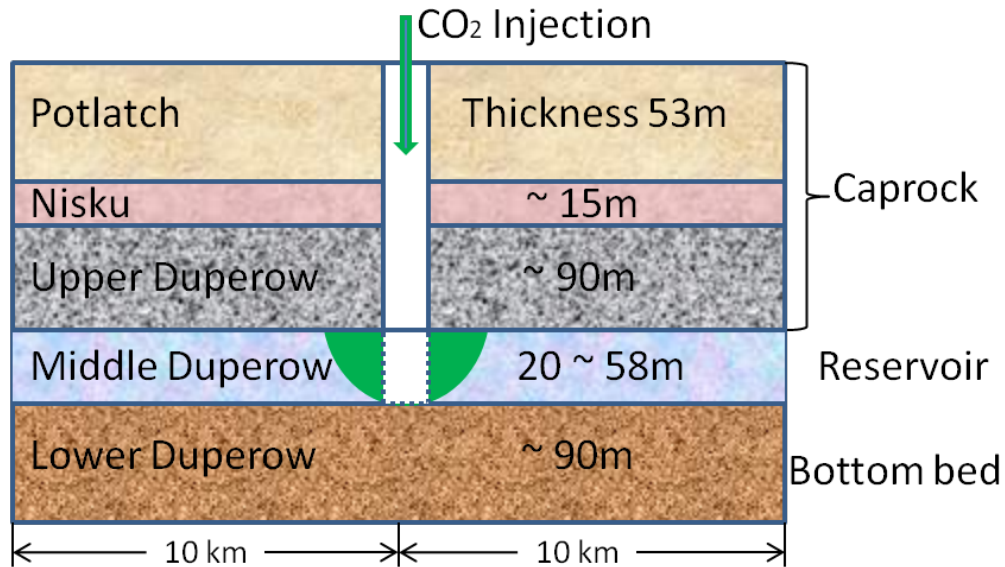
Figure 3-2: Diagrammatic cross section through 1 injection well for the numerical model of Kevin Dome site

a) Statistics of well log data

The log data from well MCFGPD-2175 has been used to define the porosity distributions in the Middle Duperow (Figure 3-3). The two log curves represent the high and low porosity data, which are shown in Figure 3-4, corresponding to two mean porosities of 0.15 and 0.08, respectively. Based on these data we convert them to permeability (Figure 3-5) according to Deng et al. (2012):

$$k=(\text{ø}/a)^3 \tag{1}$$

where k is permeability (m^2), ø is porosity and a is a constant.
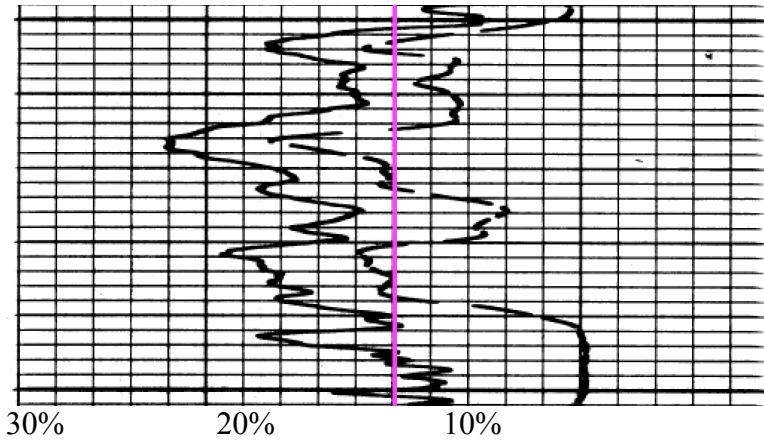
30%   20%   10%

Figure 3-3: The well log data for the middle Duperow with a thickness of 16 meters

By using the log permeability data we compute the sample semivariograms in vertical direction and fit it with an exponential function (Figure 3-6). Then we obtain the statistical parameters of the log permeability: variance of 0.25, vertical integral scale of 4.5 meters, and mean permeability of 2.51×10^{-14} m^2.

b)   Permeability field for the middle Duperow

By assuming that the horizontal integral scale is 100 times larger than the vertical one, we generate the heterogeneous permeability field for the middle Duprow with the sequential Gauss method and the permeability data (shown in Figure 3-7) as the conditional data.

c)
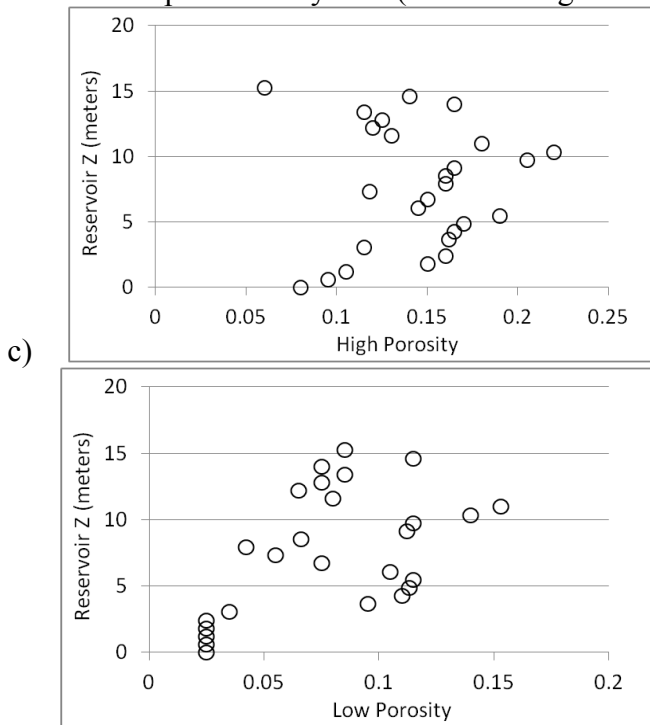
Figure 3-4: The high porosity (upper, with a mean of 0.15) and low porosity (lower, with a mean of 0.08) distributions in the middle Duperow, converted from the well log data.
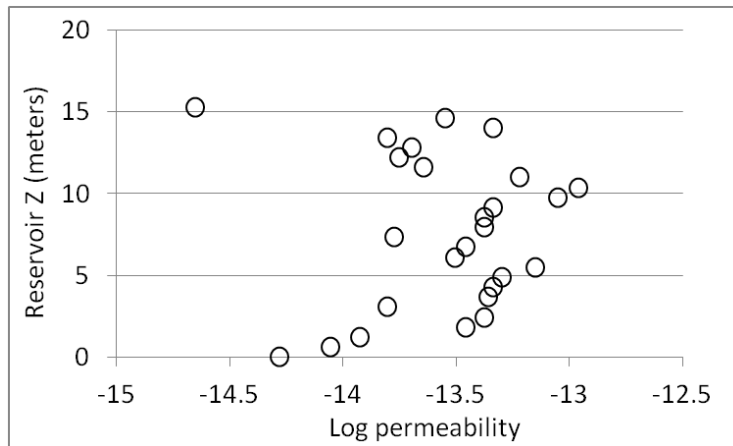
Figure 3-5: The log permeability ($\log_{10}\text{m}^2$) distributions in the middle Duperow, converted from the well log data.
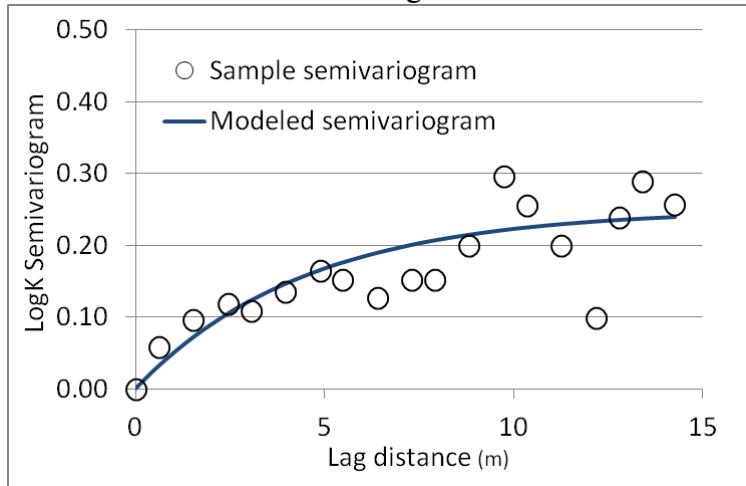

Figure 3-6: The sample semivariograms of the log permeability and the modeled results with an exponential function, a variance of 0.25 and an integral scale of 4.5 meters.
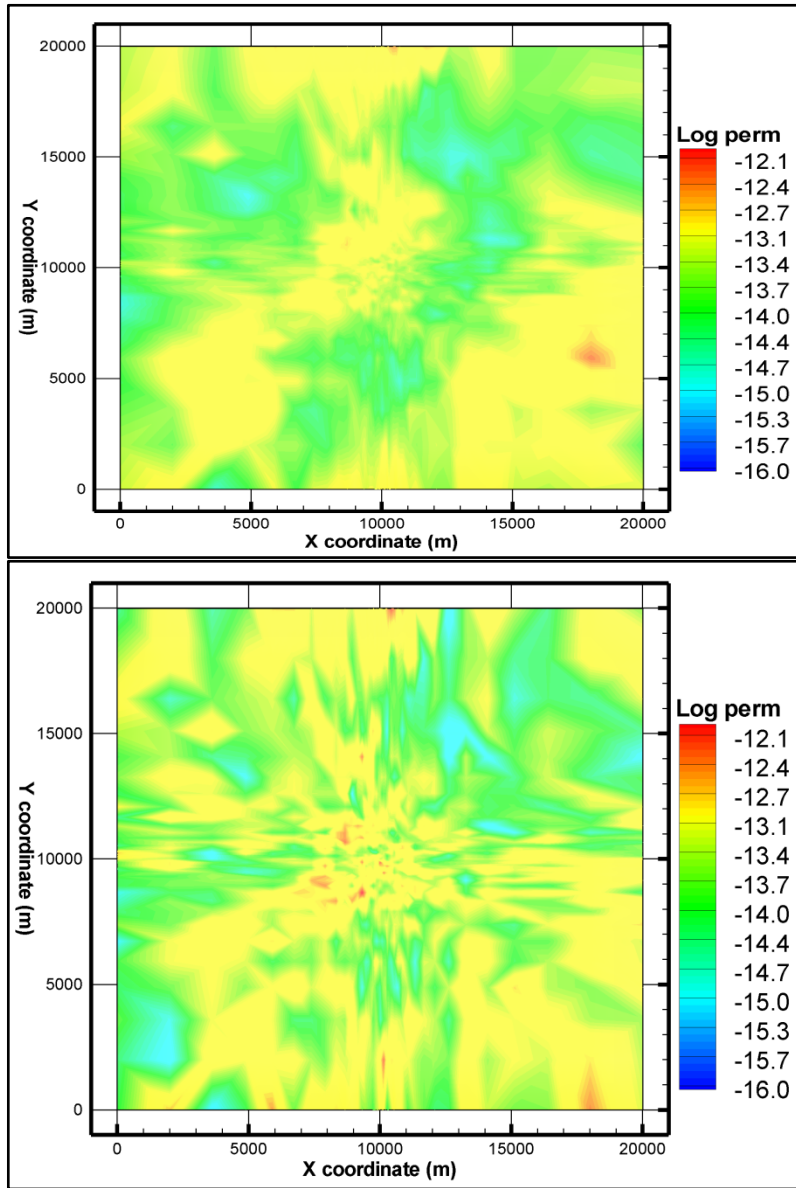
Figure 3-7A: The simulated permeability field for low porosity (0.08, upper) and high porosity (0.15, lower) for the middle Duperow reservoir in map view.
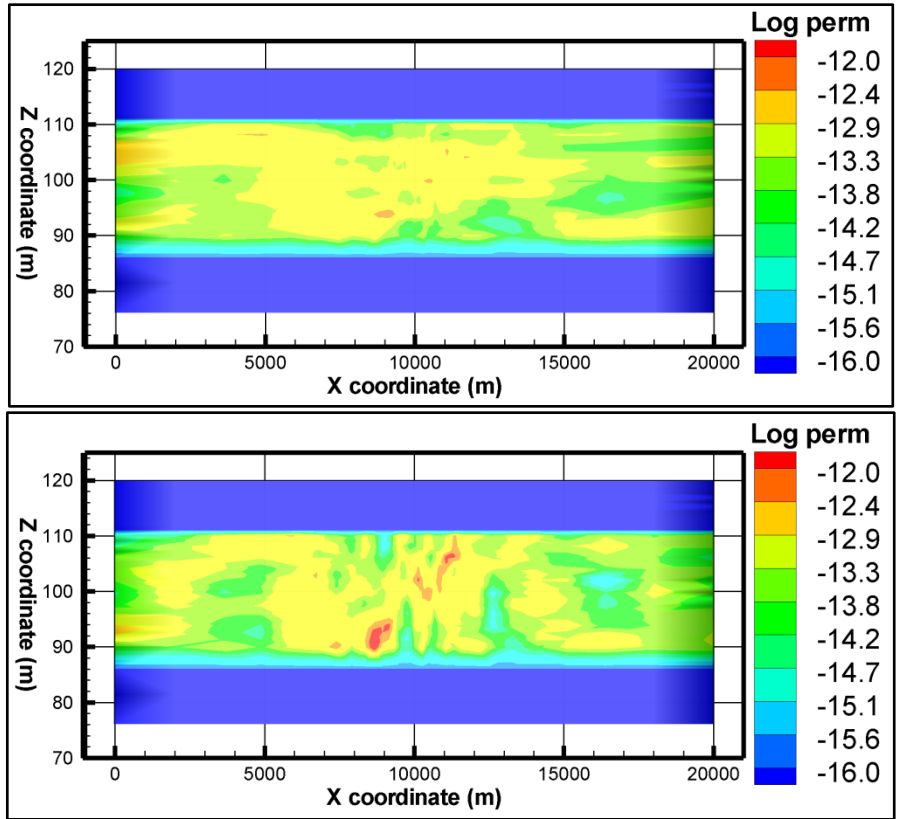
Figure 3-7B: The simulated permeability field for low porosity (0.08, upper) and high porosity (0.15, lower) for the middle Duperow reservoir in cross-section.
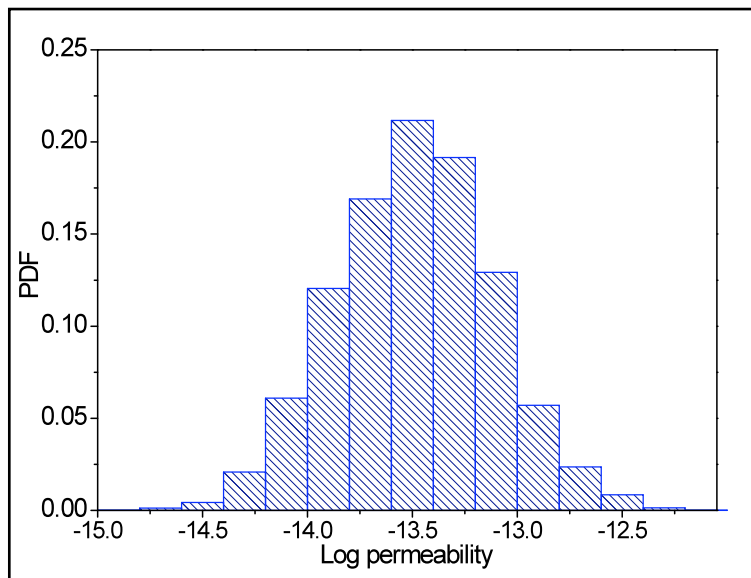

Figure 3-7C: The histogram of the generated permeability values for the middle Duperow.

a) CO_2 injection simulation

A 3-D heterogeneous numerical model is used to simulate the CO_2 flow and transport in the Kevin Dome field. The model size is 20km X 20km X 280m with 197,213 nodes. The injection well is located in the center of the model where the grid is highly refined with minimum dx, dy, dz of 3, 3, and 1 m, respectively. Away from the injection well, the numerical grids become coarse (Figure 3-8). The generated permeability field of the middle Duperow is mapped into the 3-D model using LAGRIT.
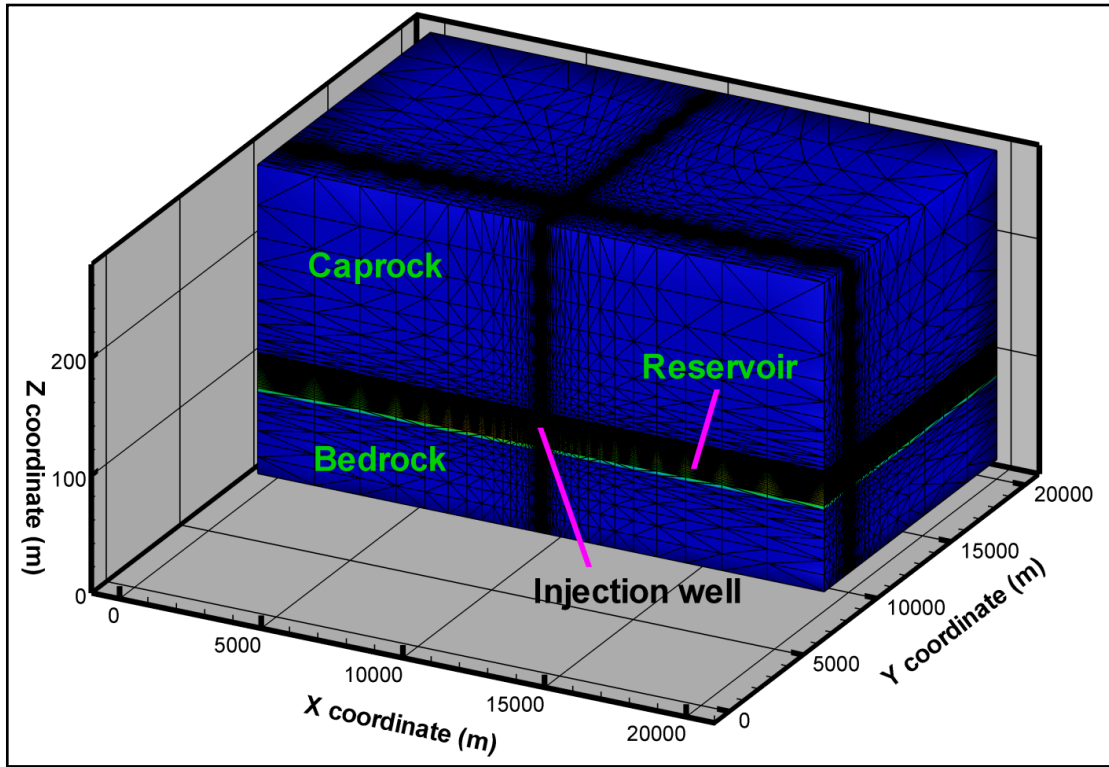

Figure 3-8: Model size and numerical grid

Figures 3-9 to 3-10 show the simulated water/CO_2 saturations in map and cross-section plots for low and high porosity/permeability field for a constant injection rate of 0.25 MT/yr. Plume radii for the examples are between 1 and 2 km, consistent with the Case 2 PENS simulations shown in Figure 2-7.
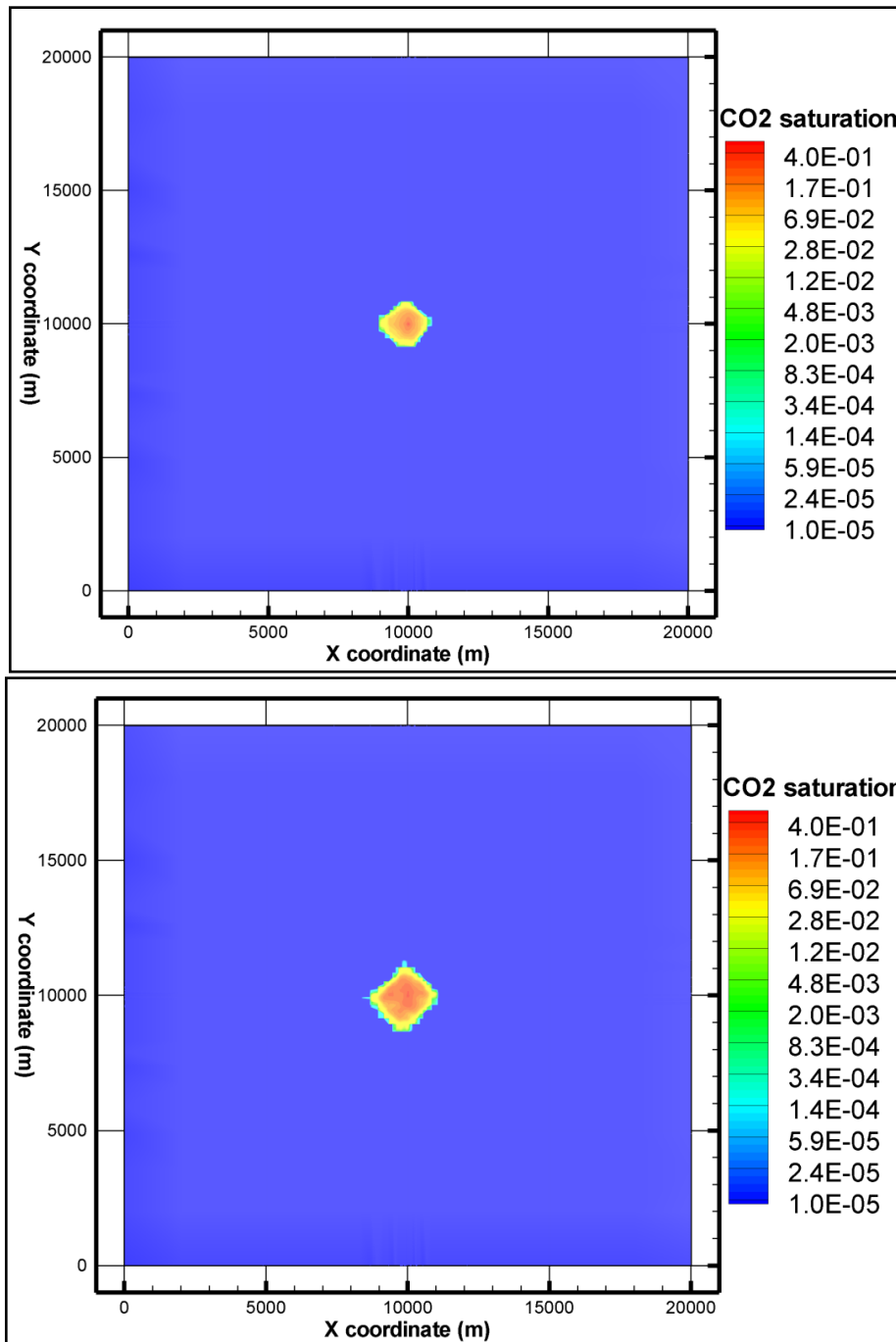
Figure 3-9: The super-critical CO₂ saturations simulated with low porosity (0.08, upper) and high porosity (0.15, lower) for the middle Duperow reservoir in map view.
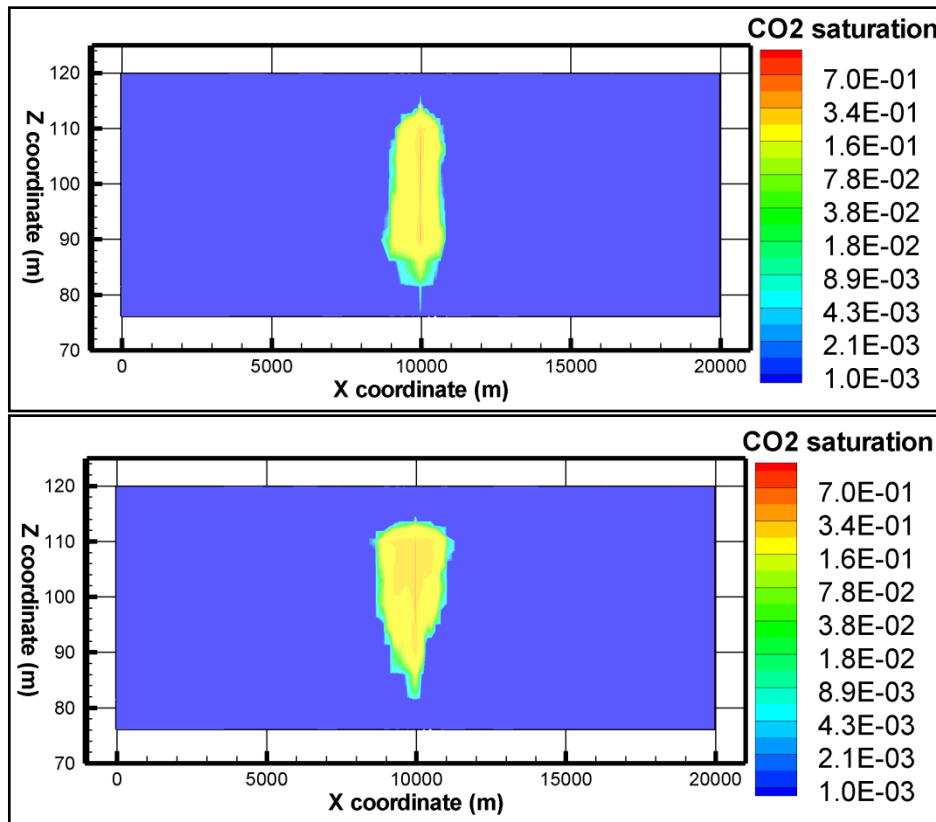
Figure 3-10: The super-critical CO_2 saturations simulated with low porosity (0.08, upper) and high porosity (0.15, lower) for the middle Duperow reservoir in cross-section.

CO_2 leakage is investigated in Figures 3-11 to 3-13 assuming that caprock and bedrock have relatively high permeability of 0.1 md. These figures compare the CO_2 leakage rates and cumulative CO_2 to the caprock and bedrock between the low and high porosity cases. In the low porosity case about 2% of the injected CO_2 leaks into the caprock and bedrock, while in the high porosity case about 4.5% of the injected CO_2 leaks into the caprock. Downward leakage in the higher porosity case is negligible because the plume moves preferentially upward due to buoyancy. Leakage into the caprock and bedrock would be lower if lower permeability was assumed for the caprock and bedrock. In Fig. 3-13, we examine how differing maximum injection pressure limits affect injection rates. A single well requires injection pressures greater than 18.5 MPa to achieve the target of 0.25 MT/yr.
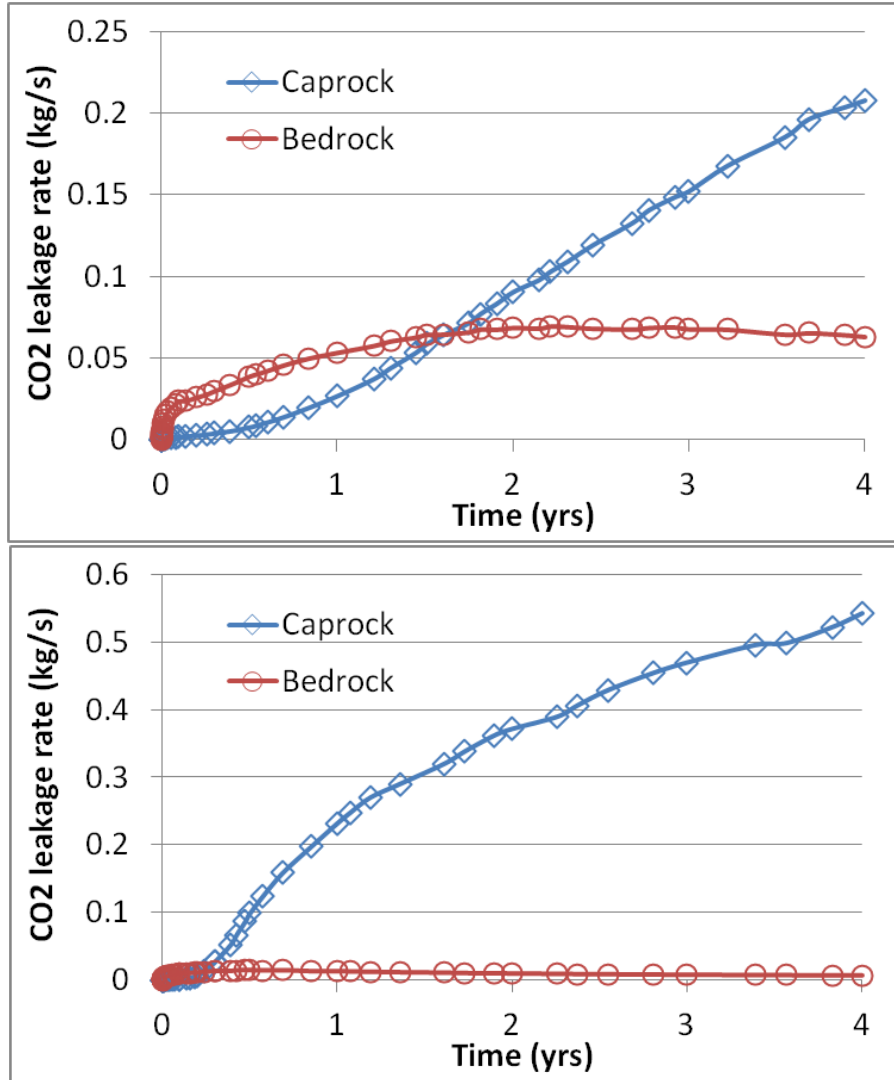
Figure 3-11: The super-critical CO_2 leakage rate (kg/s) to the caprock and bedrock simulated with low porosity (0.08, upper) and high porosity (0.15, lower).
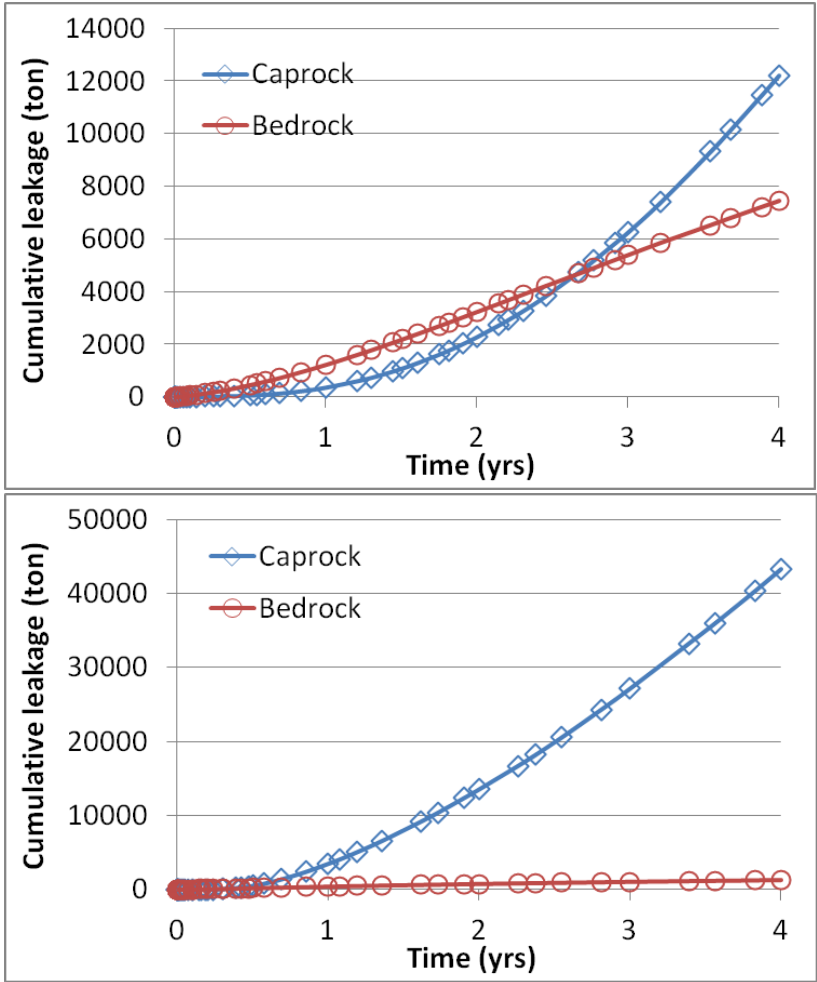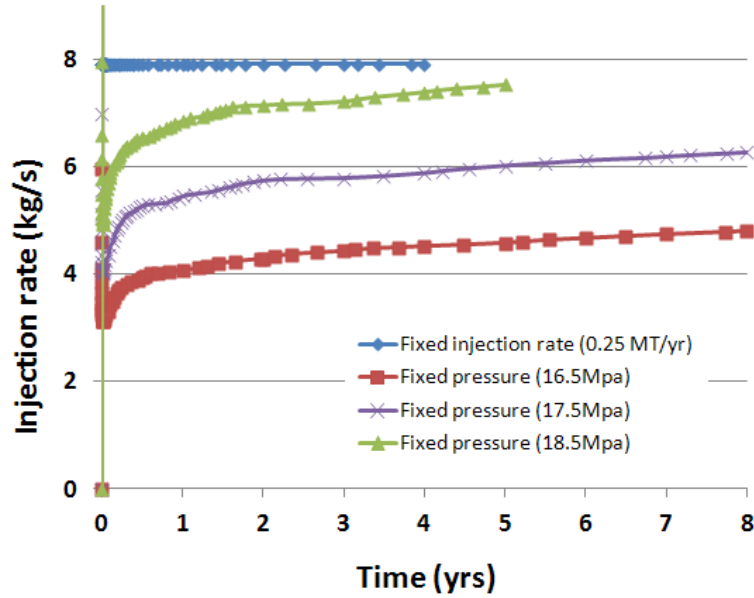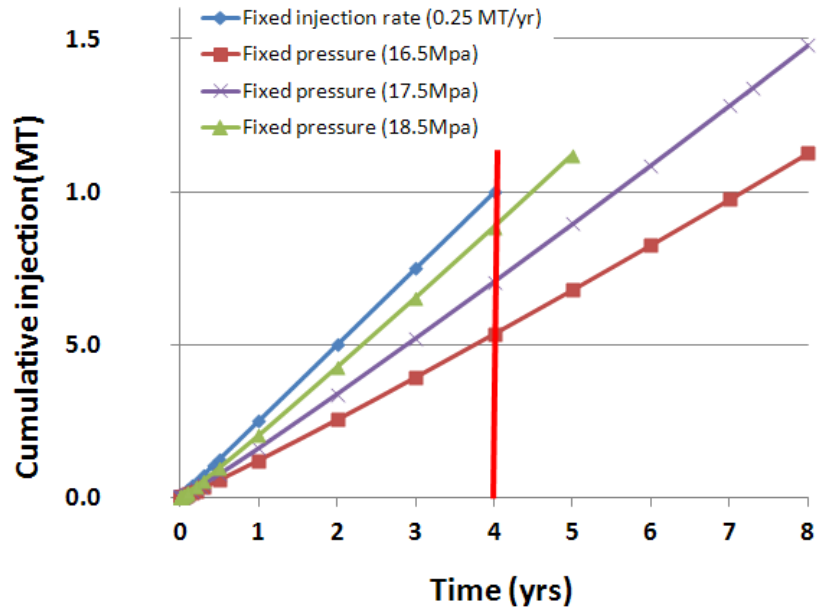
Figure 3-12: The cumulative super-critical CO_2 leaked to the caprock and bedrock simulated with low porosity (0.08, upper) and high porosity (0.15, lower).

Figure 3-13: Injection rate (A) and cumulative well injection (B) for different scenarios. The target injectivity is near 8 kg/s in (A) and the target of 4 years is shown as a red line on (B).

4. CO$_2$ Production Risk Analysis

The Kevin Dome project requires both production of CO$_2$ from the CO$_2$ gas cap and injection of CO$_2$ into the water leg. As with injection, there is uncertainty in the rate of CO$_2$ production and the number of wells required to produce at a rate of 0.25 MT/yr. CO$_2$ Production risks for the project were analyzed using analytical methods and the LANL-developed porous flow simulator FEHM. Appendix C presents model validation between FEHM and the analytical solutions. For the analysis of uncertainty, we use the analytical solutions to allow many model runs in a short period of time. FEHM is used to calculate bottom hole pressure for a range of wellhead pressures, and this information is fed back into the discussion of likely risks.

We present results for pressure drawdown as a function of reservoir properties that have uncertain values using the analytical models. Bottom hole pressure drawdown (at the well screen) has been chosen to highlight project risks of production uncertainty. One limit for bottom hole pressure is given by the requirement that the pressure in the reservoir at the well screen cannot be less than the atmospheric pressure plus the weight of a static column of CO$_2$ standing from the well screen to the wellhead (at the surface). With a column of pure CO$_2$ gas, a temperature gradient of 25 ^{o}C/km, top temperature of 10 ^{o}C, and a wellhead open to the atmosphere (P=0.1 MPa), the minimum bottom hole pressure is calculated to be 0.118 MPa. Additionally, the well engineers and transport engineers on the project will have to decide on what optimum wellhead pressure is required to ensure adequate pressure for phase change considerations within the borehole and transportation past the wellhead toward the injection site. As required wellhead pressure increases, the weight of the pure CO$_2$ column increases because density is a strong function of pressure (Figure 4-1).
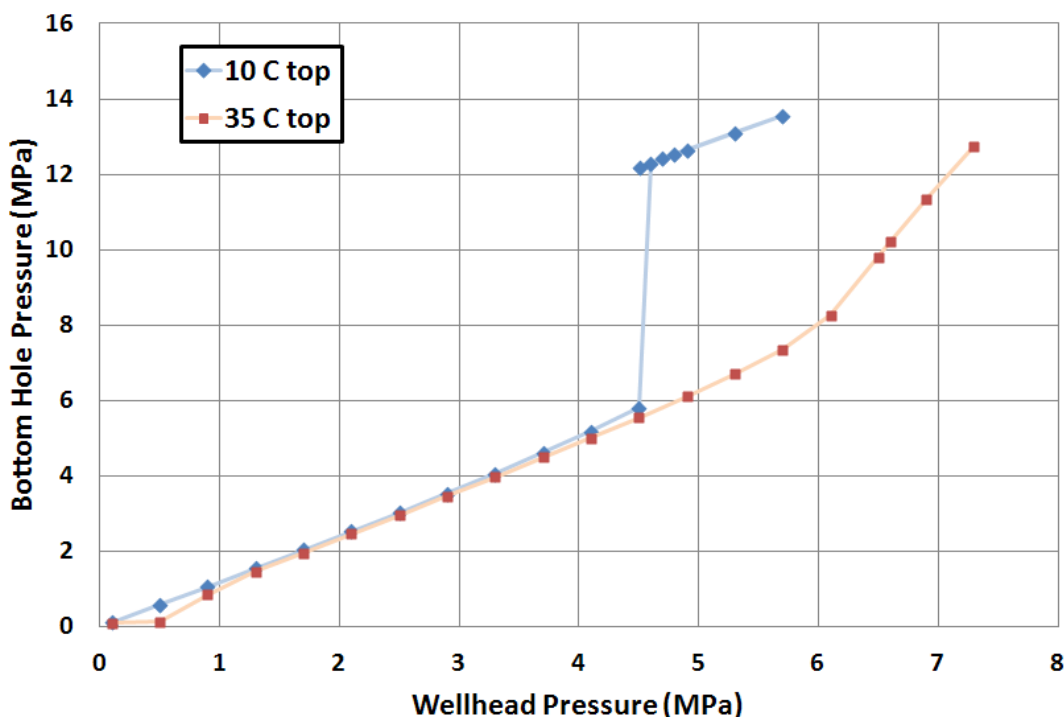
Figure 4-1. Bottom hole pressure as a function of wellhead pressure for a static column of CO_2 as calculated using FEHM.

Thus, with a wellhead pressure of 3.1 MPa, the static CO_2 bottom hole pressure is calculated (using FEHM) to be 3.8 MPa, increasing the weight of the column from 0.018 MPa to 0.7 MPa. Interestingly, at 4.5 MPa of wellhead pressure and a fixed top temperature of 10C, the entire column of CO_2 shifts from a pure gas to pure liquid and density experiences an abrupt increase leading to a similar sharp increase in bottom hole pressure. Because we do not know the target wellhead pressure at this time, we use the modeling to show how bottom hole pressure changes as a function of uncertain model variables. However, Figure 4-1 shows that the project will not be able to produce at supercritical conditions (7.3 MPa of pressure at the wellhead) or CO_2 will reverse direction and flow downward into the formation because the bottom hole pressure (12.MPa) will exceed the in-situ formation pressure (10MPa). The orange curve on this figure shows the results for a constant 35 ^{o}C column. Simulations currently in progress are showing that flow rates of 1.58 kg/s (50 kT/yr) cause cooling of the geothermal gradient to below 7 ^{o}C at the wellhead. It is likely that a single well running at 250 kT/yr would require heaters to prevent freezing at the wellhead due to Joule-Thomson cooling of the CO_2 as it decompresses (Preuss et al., 2008). Similarly, J-T heating in the injection well could lead to higher injection temperatures than those found at the wellhead.

Uncertain variables explored in the analysis of pressure drawdown include: thickness, permeability, porosity, and production rate. Figure 4-2 shows drawdown sensitivity to production interval thickness. For a thicker section with mean permeability near 25 md (Case 1), a pressure drop of less than 1 MPA will lead to flow on the order of 50,000 tons/yr for thickness between 10 and 30 m. This rate was chosen based on the project goal to have no more than 5 production wells that can produce one million tons in 4 years. When the rate is doubled for this case to 100,000 tons/yr, downhole pressure drops range between 1 and 2 MPa over the same range of uncertain thicknesses. Production from thin, higher permeability units (Case 2) leads to more significant drawdown, with the thinnest (2m) layers resulting in more than 6 MPa of drawdown at the well screen.

	Thickness h (m)		Permeability k (m2)		Porosity ϕ	
	$<h>$	σ_h	$<logk>$	σ_{logk}	$<\phi>$	σ_ϕ
Case 1	20	3	-13.5458	0.141	0.1	0.01
Case 2	3	0.3	-13.0485	0.205	0.2	0.01

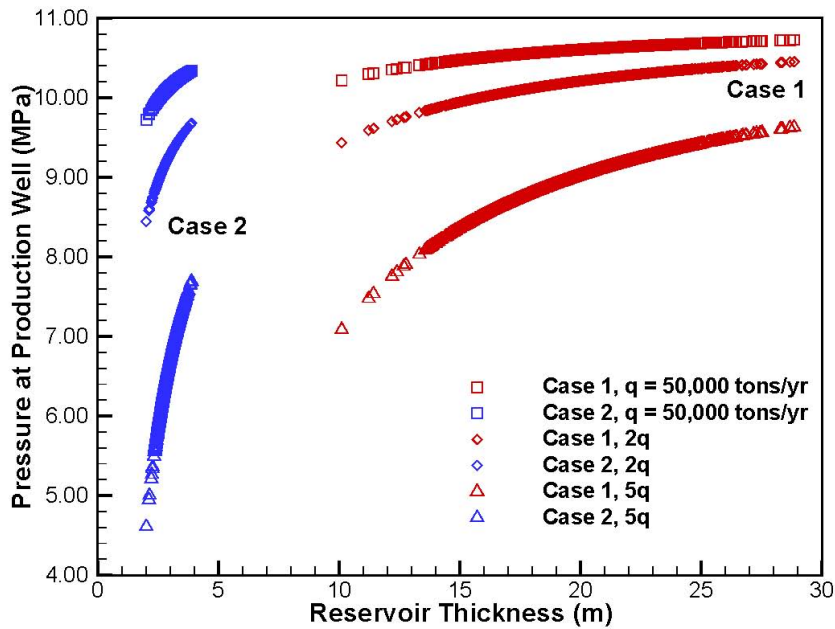Table 4-1 Parameter uncertainty for production analysis

Figure 4-2. Dependence of CO_2 pressure at the production well on the reservoir thickness and production rate.

Figure 4-3 shows modeled drawdown sensitivity to permeability. Interestingly, target production rates can be achieved below 10 md, a value at least a factor of 5 lower than the permeability required for the target injection interval. The lower required permeability is due to the lower flow rates needed on each production combined with the fully CO_2 saturated production interval having a higher effective gas phase mobility.
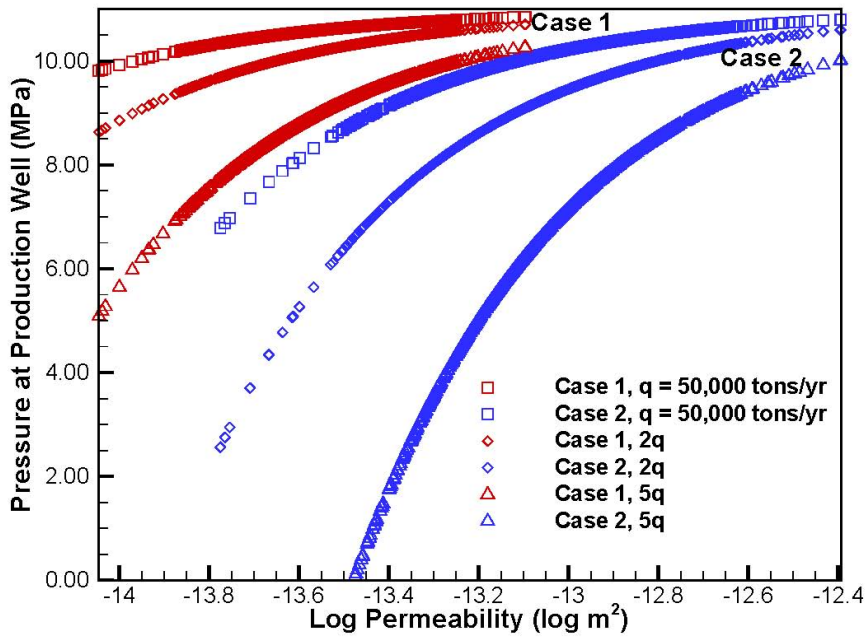
Figure 4-3. Dependence of CO_2 pressure at the production well on the reservoir thickness and production rate.

Figure 4-4 shows modeled drawdown sensitivity to porosity. Not surprisingly, porosity has only a second order effect compared to thickness, permeability, and production rate.

The final point of this section is that given the bottom hole pressure constraint from Figure 6 of less than 6 MPa, most variations in uncertainty in the current analysis lead to acceptable production rates and little risk to the project. Only in extreme cases where high volumes (0.25 MT/yr) are extracted from a thin or low permeability layers do bottom hole pressures fall below reasonable values.
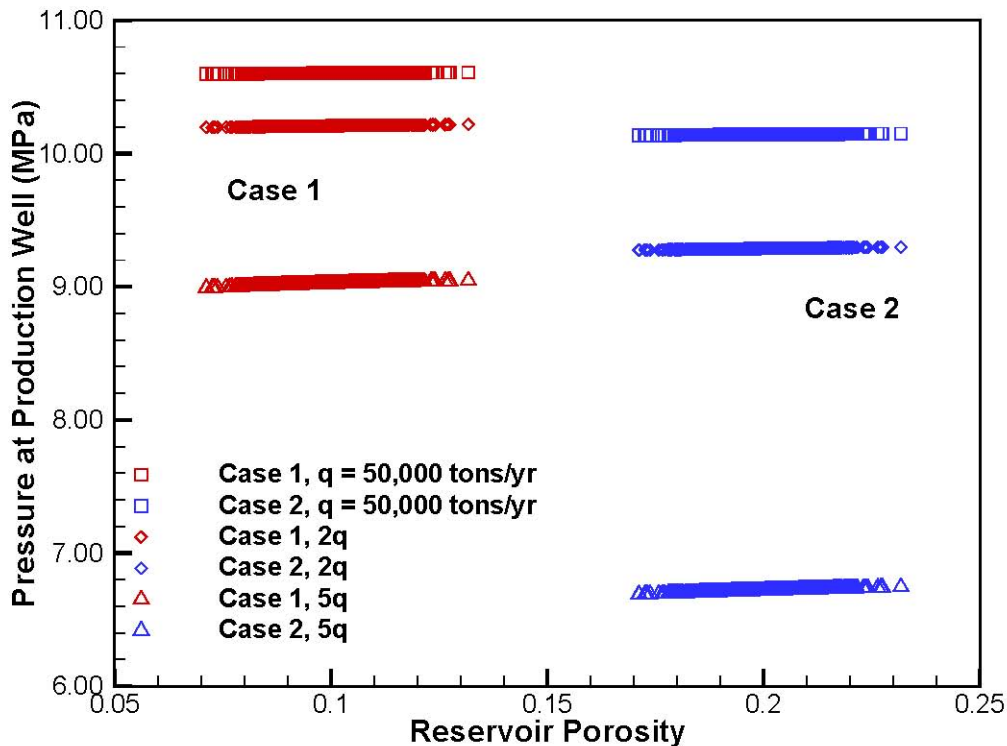
Figure 4-4. Dependence of CO_2 pressure at the production well on the reservoir porosity and production rate.

5. Subsurface Risk Path Forward

Plans for carrying the project forward include 1) further analysis of heterogeneity including density inversion results from the 3-D seismic data when they become available; 2) use of the heterogeneous plume estimates to delineate project risk associated with monitoring well locations; 3) more production analysis to include heterogeneity and Joule-Thomson cooling within the production wells; 4) Full 3-D CO_2-PENS simulations to calculate leakage risks associated with existing wells; and 5) Groundwater impacts from such leakage.

Figure 5-1 shows a schematic of a plan to implement a reduced order model of plume shape and size based on a set of 3-D reservoir simulations. This approach may allow us to more quickly answer risk questions as more data becomes available on ranges of parameter uncertainty.

PSUADE will be used to sample the uncertain parameters to form a number of realizations (for example 500 realizations). Due to the variations of the sampled reservoir thickness, we need to generate different grids for different realizations. The main output variables are CO_2 injection capacity, CO_2 plume sizes, and CO_2 leakage rates from the caprock. The response surfaces of

these three output variables will be generated using PSUADE. A list of some of the anticipated tasks is as follows:

- Generate 300 3-D heterogeneous models with PSUADE by using the data listed in Table 3-2;
- Conduct Monte Carlo simulations with FEHM to evaluate the mean, 5% and 95% percentile of CO_2 plume size (dx, dy, dz) in x,y,and z directions, 4-year injection rate (r4), leakage rates to caprock (rc) and bedrock (rb), and Area of Review (Aor) to the underground sources of drinking water (USDW);
- Conduct global sensitivity analysis of the output valiables to the input parameters to define the most important variables with PSUADE;
- Develop the reduced order models (ROMs) for the major output variables (dx, dy, dz, r4, rc, rb, Aor) with PSUADE; and
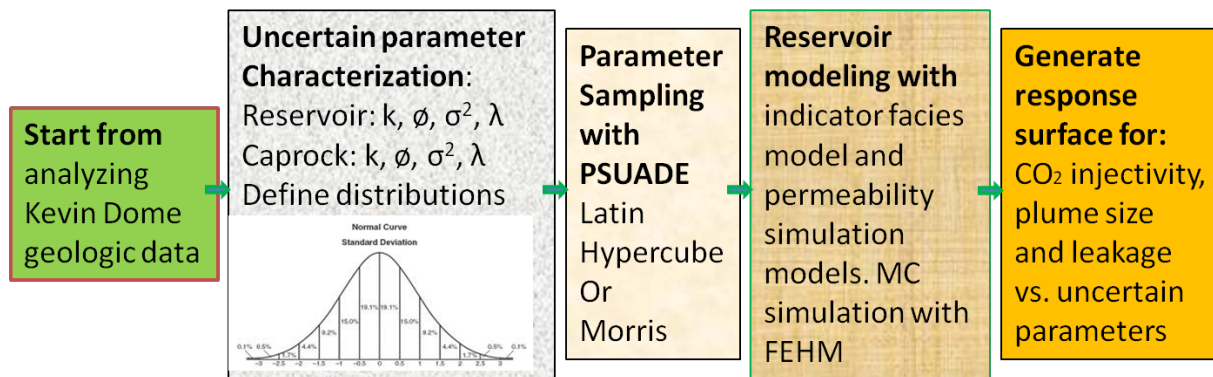- Input the ROMs to CO_2-PENS for risk assessment

Figure 5-1: Workflow description of uncertainty quantification and the development of response surfaces with PSUADE (Problem Solving environment for Uncertainty Analysis and Design Exploration, Tong et al., 2011).

6. **References**

Deng, H., P.H. Stauffer, Z. Dai, Zunsheng Jaio, R.S. Surdam, Simulation of Industrial-Scale CO2 Storage: Multi-Scale Heterogeneity and its Impacts on Storage Capacity, Injectivity and Leakage, *Int. J. Greenhouse Gas Control*, Volume 10, September 2012, Pages 397–418 . http://dx.doi.org/10.1016/j.ijggc.2012.07.003

Eggie, L., Chow, N. and Nicolas, M.P.B. Sedimentology of the Wymark Member (middle unit) of the Upper Devonian Duperow Formation, southwestern Manitoba (NTS 62F14, 15, 16); in Report of Activities 2012, Manitoba Innovation, Energy and Mines, Manitoba Geological Survey, p. 160–171, 2012.

Tong, C., PSUADE User's Manual (Version 1.2.0), LLNL-SM-407882, Lawrence Livermore National Laboratory, Livermore, CA 94551-0808, May, 2011.

Keating, G.N., Middleton, R.S., Stauffer, P.H., Viswanathan, H.S., Letellier, B.C., Pasqualini, D., Pawar, R.J., Wolfsberg, A.V., 2011a. Mesoscale Carbon Sequestration Site Screening and CCS Infrastructure Analysis. Environmental Science & Technology 45, 215-222.

Nordbotten, JM; Celia, MA; Bachu, S (2005). Injection and storage of CO_2 in deep saline aquifers: Analytical solution for CO_2 plume evolution during injection, *Transport Porous Med.* **2005***, 58*, 339-360.

Preuss, K., On CO_2 fluid flow and heat transfer behavior in the subsurface, following leakage from a geologic storage reservoir, Environ. Geol., 54:1677-1686, 2008.

Stauffer, P.H., Viswanathan, H.S., Pawar, R.J., Guthrie, G.D., 2009b. A system model for geologic sequestration of carbon dioxide. Environmental Science and Technology 43, 565-570.

Viswanathan, H.S., Pawar, R.J., Stauffer, P.H., Kaszuba, J.P., Carey, J.W., Olsen, S.C., Keating, G.N., Kavetski, D., Guthrie, G.D., 2008. Development of a hybrid process and system model for the assessment of wellbore leakage at a geologic CO_2 sequestration site. Environmental Science & Technology 42, 7280-7286.

Zyvoloski, G.A., Robinson, B.A., Dash, Z.V. and Trease, L.L. (2011) Summary of the Models and Methods for the (FEHM) Application --- A Finite-Element Heat- and Mass-Transfer Code. LA-13306-MS, Los Alamos National Laboratory, Los Alamos, New Mexico.

White MD and M. Oostrom, STOMP, Subsurface Transport Over Multiple Phases, User's Guide, V4.0, PNNL-15782, Pacific Northwest National Laboratory, Richland, Washington 99352, 2006.

Appendix A

Schlumberger Tables 11-13 from the expert elicitation Kevin Dome Project Initial Risk Assessment initially done from June-Oct 2011.

FEP Title	Sbg	Lbg	Riski	Rank
Schedule and planning	2.94	3.06	9.3	1
On-road driving	3.00	3.37	9.0	2
CO_2 Delivery System: Source Composition	3.00	3.00	9.0	3
Legal/regulatory: lawsuits	3.15	2.70	8.5	4
CO_2 injectate effects: Groundwater contamination: Public perception	3.21	2.93	8.5	5
Contracting	2.93	3.13	8.4	6
Placement and Performance of Production Wells	3.16	2.63	8.4	7
Reservoir injectivity	2.75	3.00	8.3	8
Legal/regulatory: Permits: Drilling and injection	3.05	3.10	8.2	9
Undefined specifications	3.00	2.67	8.0	10
Startup/shutdown operations	2.50	3.00	8.0	11
Characterization: Ability to characterize reservoir	2.33	3.00	8.0	12
Workover	2.00	4.00	8.0	13
Seismicity (project-induced earthquakes)	2.67	2.33	7.7	14
Construction and operations activities (project) other than drilling	2.50	3.00	7.5	15
Legal/regulatory: Area of review	2.89	2.47	7.5	16
Accidents and unplanned events (project)	2.75	2.65	7.5	17
Adequate risk characterization	3.00	2.40	7.4	18
Legal/regulatory framework	3.00	2.33	7.3	19
Staffing and staff competency	2.50	2.81	7.3	20

Table 1. Top 20 ranked FEPs by average individual S*L (Risk i) value

Upper-bound Severity ("S_{ub}") data

The FEP ranking shown in the above Table11 is based on the product $S_{bg} * L_{bg}$. This quantity estimates the likelihood that events entailing the "best-guess" consequence severities will occur. While it is clearly important to manage the larger "best guess" risks, it is also important to manage the project's exposure to the "upper-bound" or "worst-case" severities. Although the likelihood that worst-case scenarios will be encountered is low by definition, this likelihood is also inherently impossible to estimate accurately. Therefore it is important to take account of and potentially to manage the risk from FEPs whose S_{ub} was rated high, regardless of likelihood. Table 12 shows the top 29 FEPs (all those having Sub = 4.0 or greater), as ranked by upper-bound Severity alone (values limited to those given by qualified participants per FEP). With this information, the project manager can evaluate resource allocation toward reducing particular high-consequence risks. In general, preferred measures to reduce risk from high-Severity events will often be *to improve the project's robustness to consequences*, rather than to attempt to

reduce the already-low probabilities. Ensuring a project's robustness to consequences is often accomplished through designing and resourcing contingency plans.

FEP Title	Sub	Rank
Construction and operations activities (project) other than drilling	5.0	1
Off-road driving	5.0	2
Legal/regulatory framework	4.7	3
Asphyxiation	4.5	4
Support from Government - political basis	4.5	5
Legal/regulatory: lawsuits	4.4	6
Working in confined areas	4.4	7
Legal/regulatory property rights and trespass	4.3	8
Adequate risk characterization	4.3	9
Reservoir injectivity	4.3	10
CO_2 injectate effects: Groundwater contamination: Public perception	4.2	11
On-road driving	4.2	12
Baseline studies	4.1	13
Placement and Performance of Production Wells	4.0	14
Support from Government - technical basis	4.0	15
CO_2 Delivery System: Source Composition	4.0	16
Seismicity (project-induced earthquakes)	4.0	17
Near-surface aquifers and surface water bodies: public perception	4.0	18
Reservoir porosity	4.0	19
Closure and sealing of boreholes	4.0	20
Legal/regulatory: CO2 ownership	4.0	21
Pressure: Reservoir overpressuring	4.0	22
Drilling and well completion (project): Blowouts	4.0	23
Caprock or confining formation: Primary	4.0	24
Pressure effects on caprock	4.0	25
Contamination of groundwater	4.0	26
Caprock geochemical properties	4.0	27
Legal/regulatory: Protected Waters definition	4.0	28
Seal failure	4.0	29

Table 2. Top 29 ranked FEPs by upper-bound Severity alone.

S_{ub} ranking and "Black Swan" FEPs

S_{ub} ranking of FEPs is based on the average of all qualified S_{ub} values given in respect to a particular FEP. FEPs involved in scenarios that are unlikely, yet very consequential, are labeled "Black Swan" FEPs after the concept of Taleb [5]. Using available FEP-evaluation data, one way to identify Black Swan FEPs is to seek exceedance of S_{ub} ranking over S*L ranking. The FEPs having the largest exceedance of S_{ub} ranking over S*L ranking (based on qualified evaluations) are identified in Table 13. Of these FEPs, two (yellow highlight) occur on neither the top-20 S*L nor the top-29 S_{ub} ranking list. Impacts from any of these "Black Swan" FEPs could come as more of a surprise because of their otherwise moderate rank.

FEP Title	RANK by S*L	RANK by Sub	Delta
Legal/regulatory: Protected Waters definition	125	28	-97
Seal failure	126	29	-97
Off-road driving	93	2	-91
Caprock geochemical properties	103	27	-76
Contamination of groundwater	94	26	-68
Legal/regulatory property rights and trespass	75	8	-67
Fractures and faults open pathway	118	61	-57
Caprock or confining formation: Primary	76	24	-52
Pressure effects on caprock	77	25	-52
Drilling and well completion (project): Blowouts	74	23	-51
CO_2 injectate: Gases besides CO_2 and water	95	46	-49
Pressure: Reservoir overpressuring	69	22	-47

Table 3. "Black Swan" FEPs, computed as ranking difference between S_{ub} and S*L.

Appendix B: Test of the grid resolutions
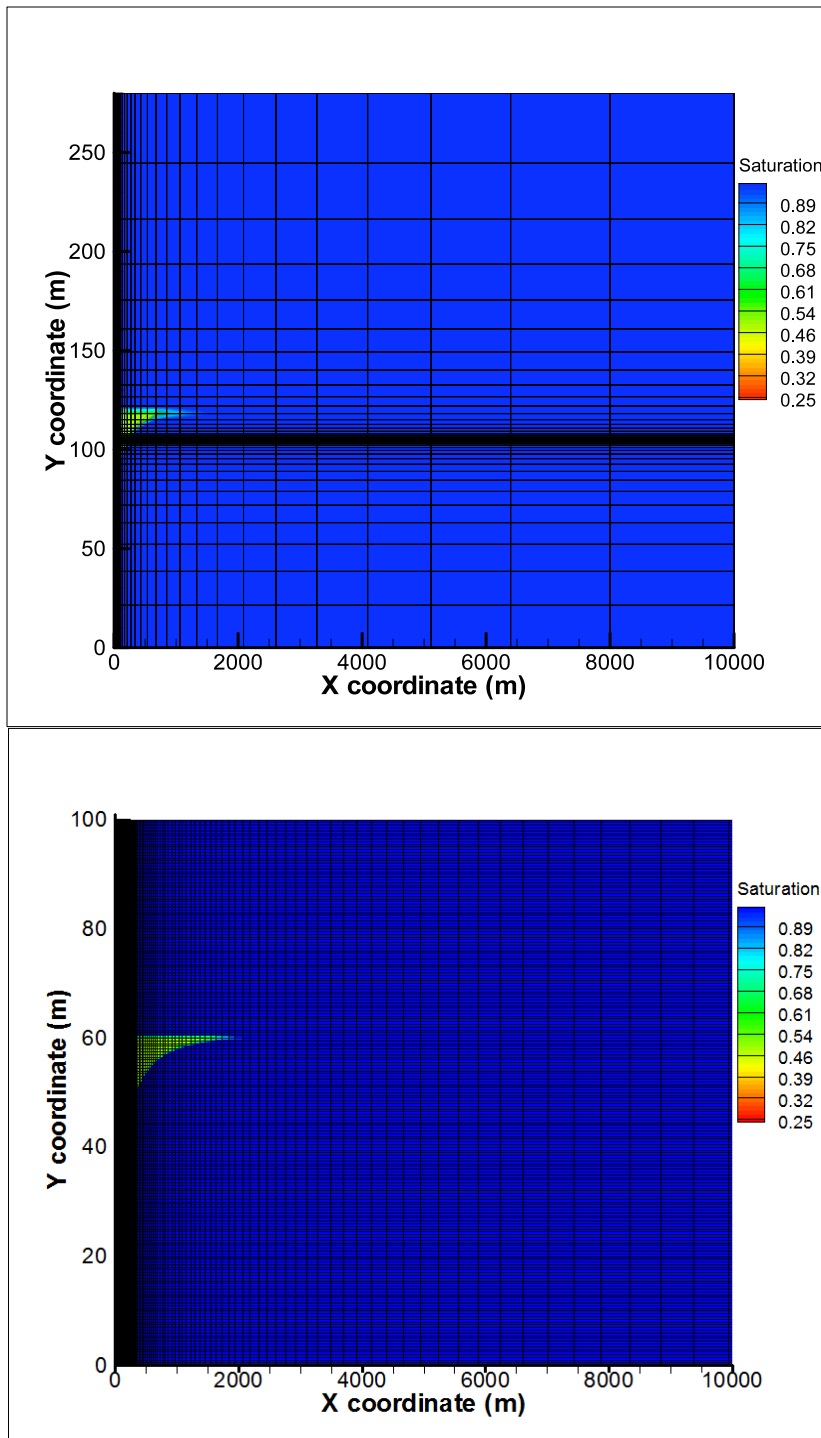### 1. 2-dimensional radial model with coarse grids

Figure B1: Comparison of the simulated water saturations of the new 2D-radial model (coarse grid, upper, with 1209 nodes) with original model (lower, with 40401 nodes).
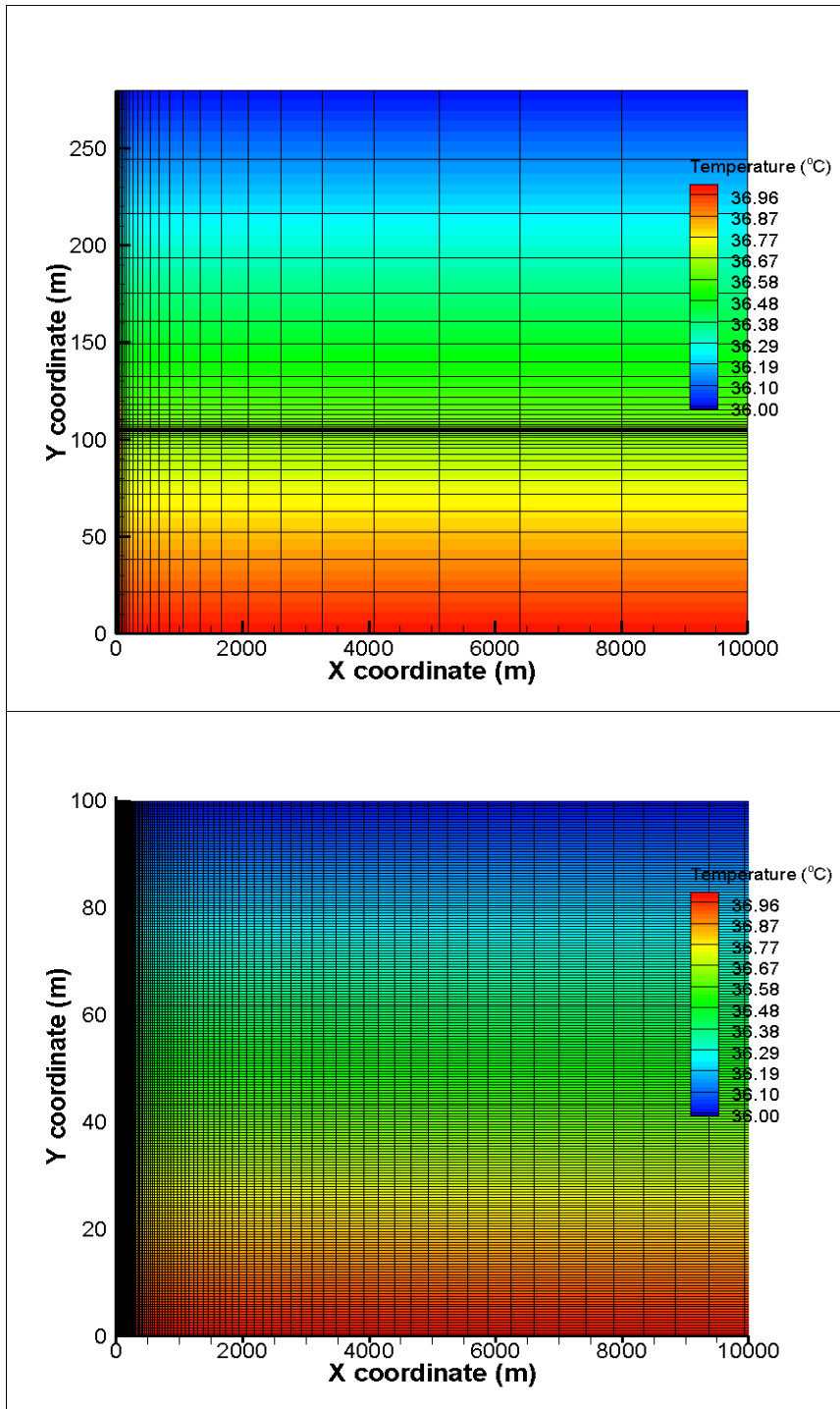
Figure B2: Comparison of the simulated temperatures of the new 2D-radial model (coarse grid, upper, with 1209 nodes) with original model (lower, with 40401 nodes).
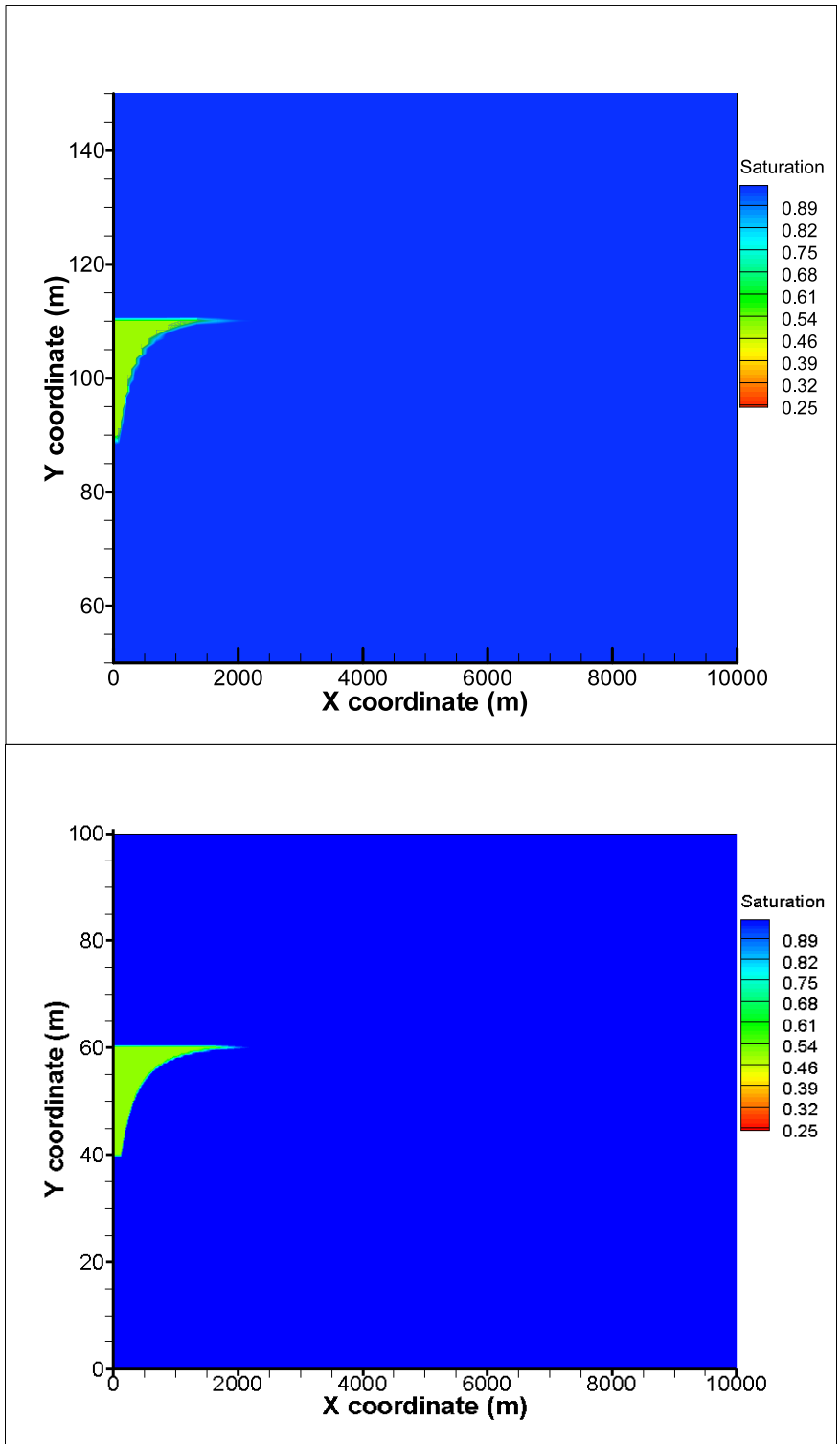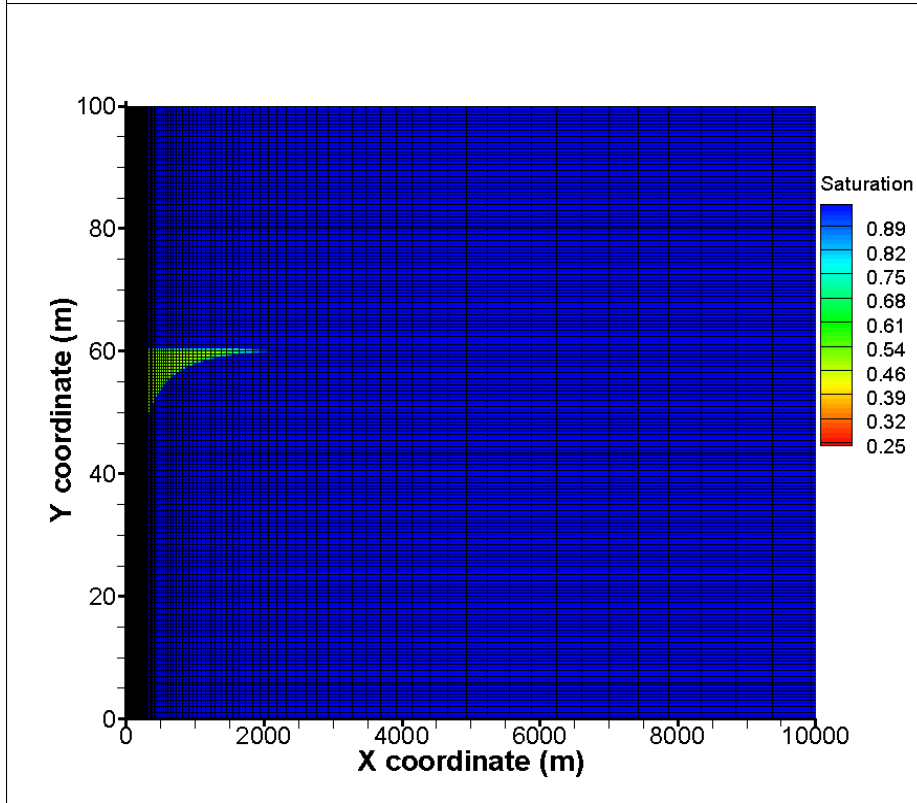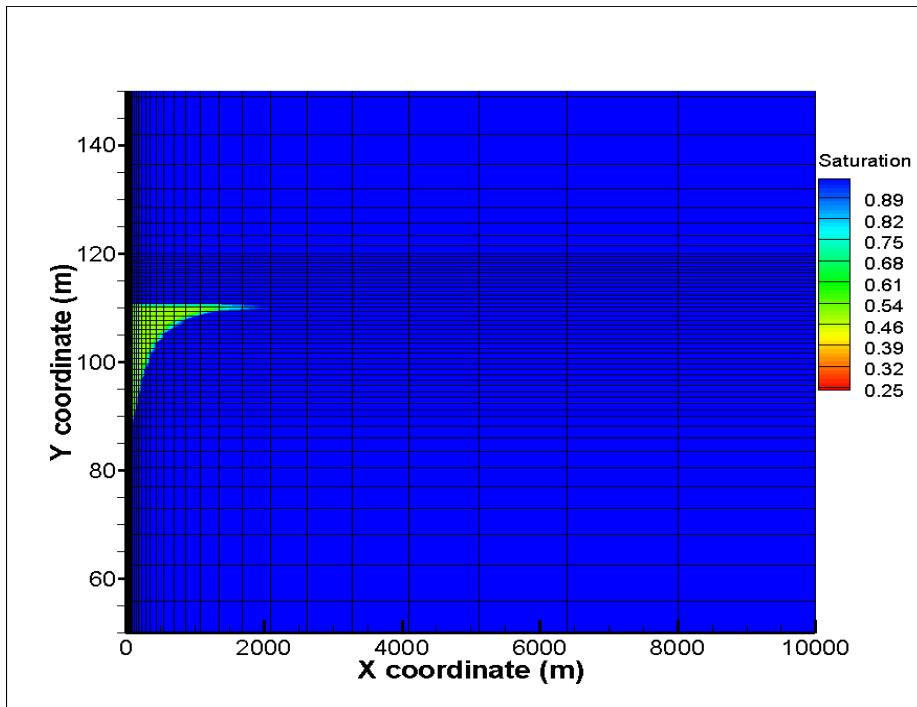
2. 2-dimensional radial model with finer grids

Figure B3: Comparison of the simulated water saturations of the new 2D-radial model (fine grid, upper, with 3366 nodes) with original model (lower, with 40101 nodes).

Figure B4: Comparison of the simulated water saturations of the new 2D-radial model (fine grid, upper, with 3366 nodes) with original model (lower, with 40401 nodes). Permeability in the caprock and bottom bed is equal to 10^{-19} m^2.
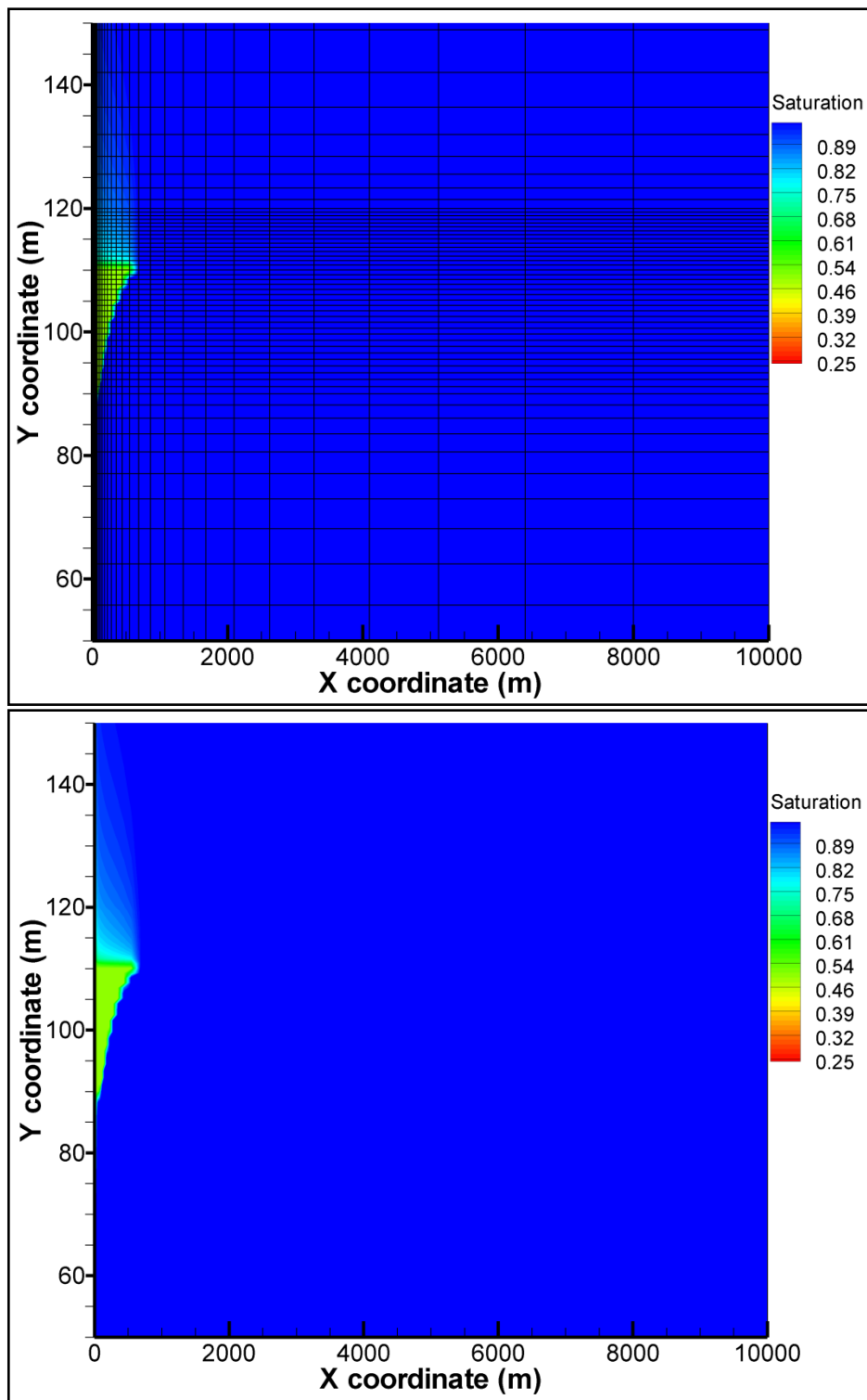
Figure B5: The simulated water saturations of the new 2D-radial model (fine grid, upper, with 3366 nodes) with a permeability in the caprock and bottom bed equal to 10^{-15} m^2.

3. 3-dimensional uniform model
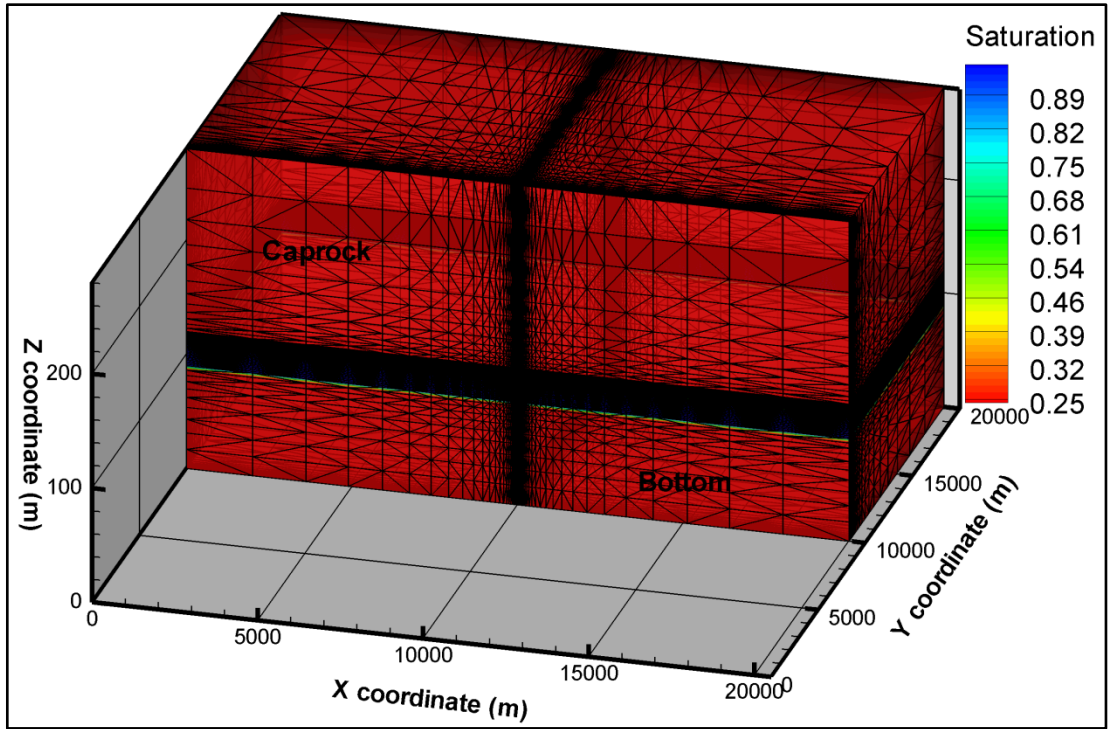
Figure B6: Model size and numerical grid
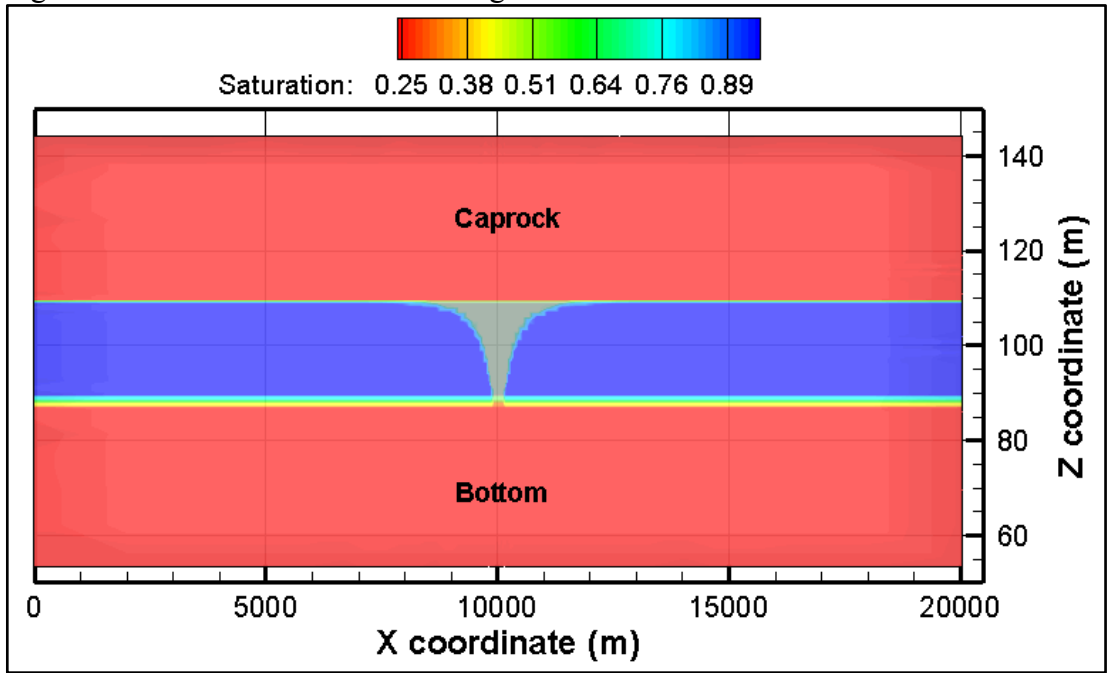
Figure B7: A cross section (at y=10000 m) shown the simulated CO_2 plume in the middle Duperow formation (no flow in the caprock and bottom bed).
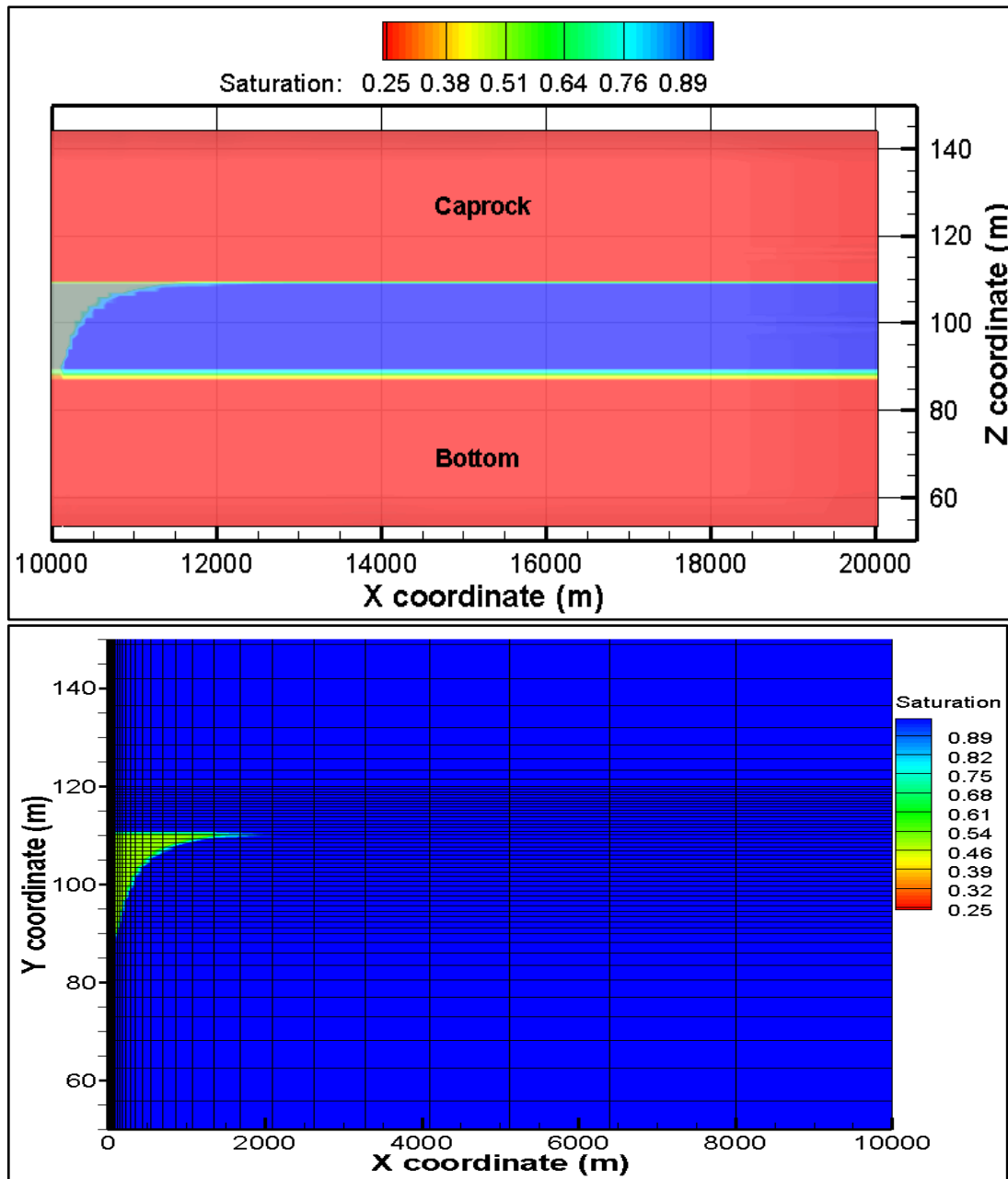
Figure B8: Comparison of the simulated CO_2 plume from the 3D model (upper, no flow in the caprock and bottom bed) with the fine 2-D radial model (lower, with 3366 nodes).
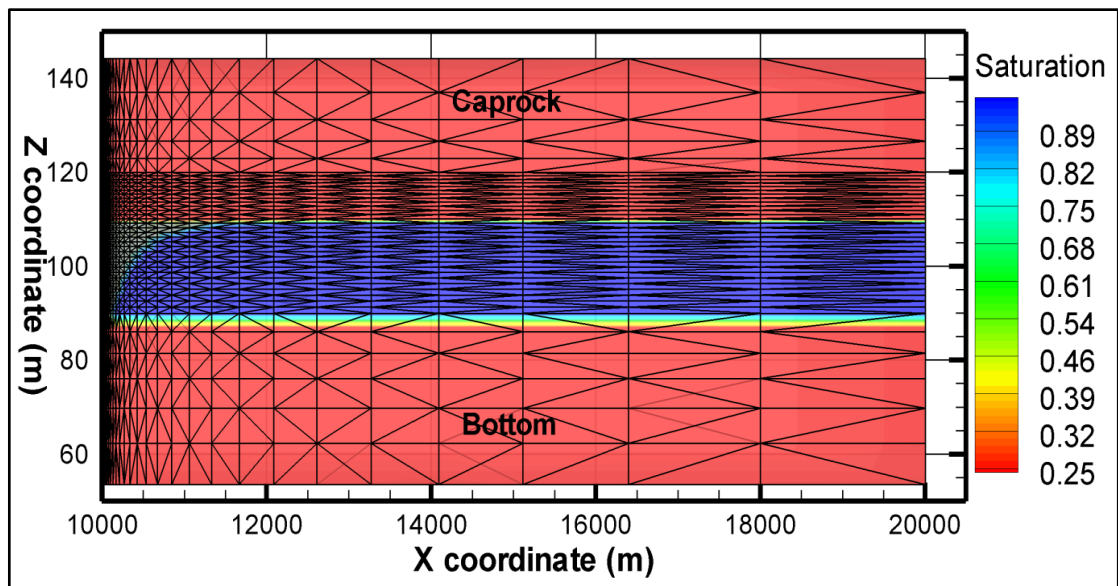
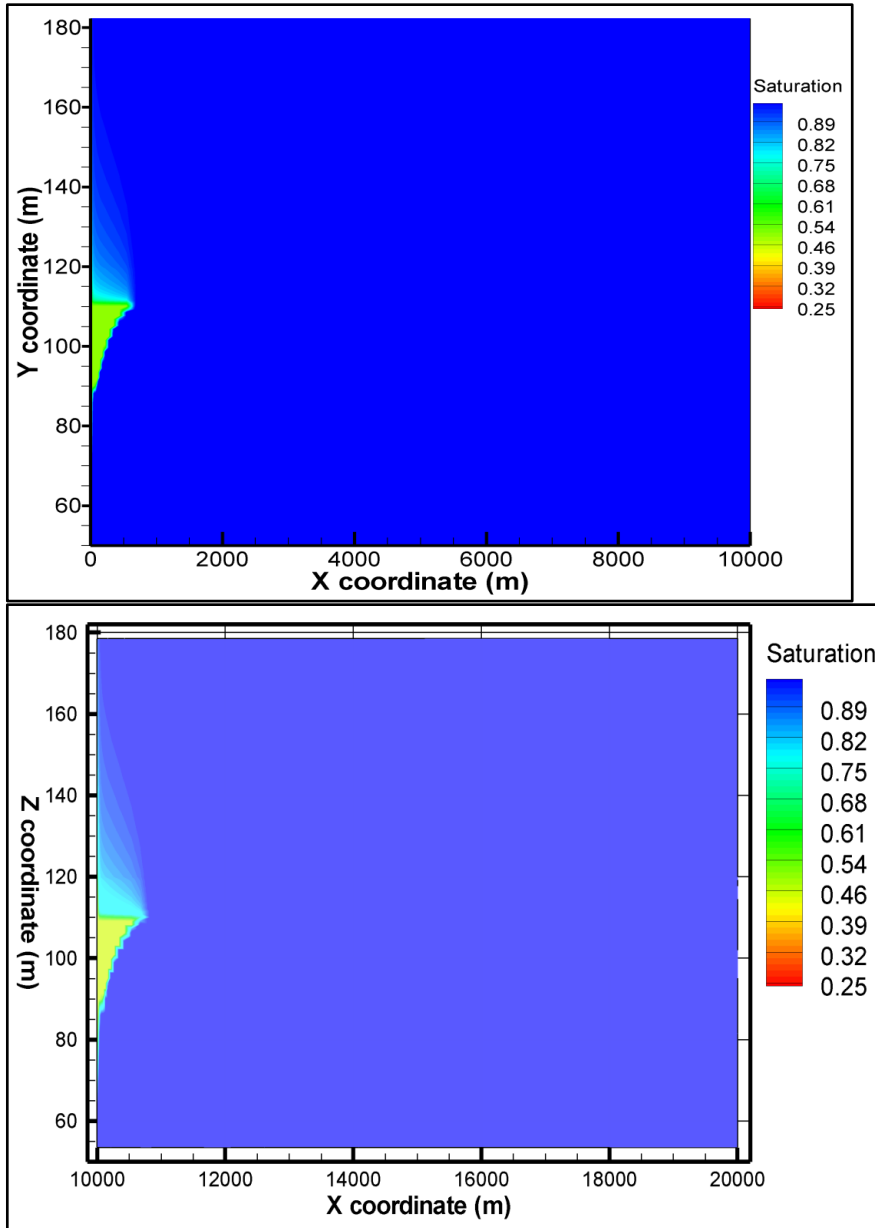Figure B9: The numerical mesh and the simulated CO_2 plume at the cross section of y=10000m.

Figure B10: Comparison of the simulated water saturations of the new 2D-radial model (fine grid, upper, with 3366 nodes) with the 3D model. Permeability in the caprock and bottom bed is equal to 10^{-15} m^2.
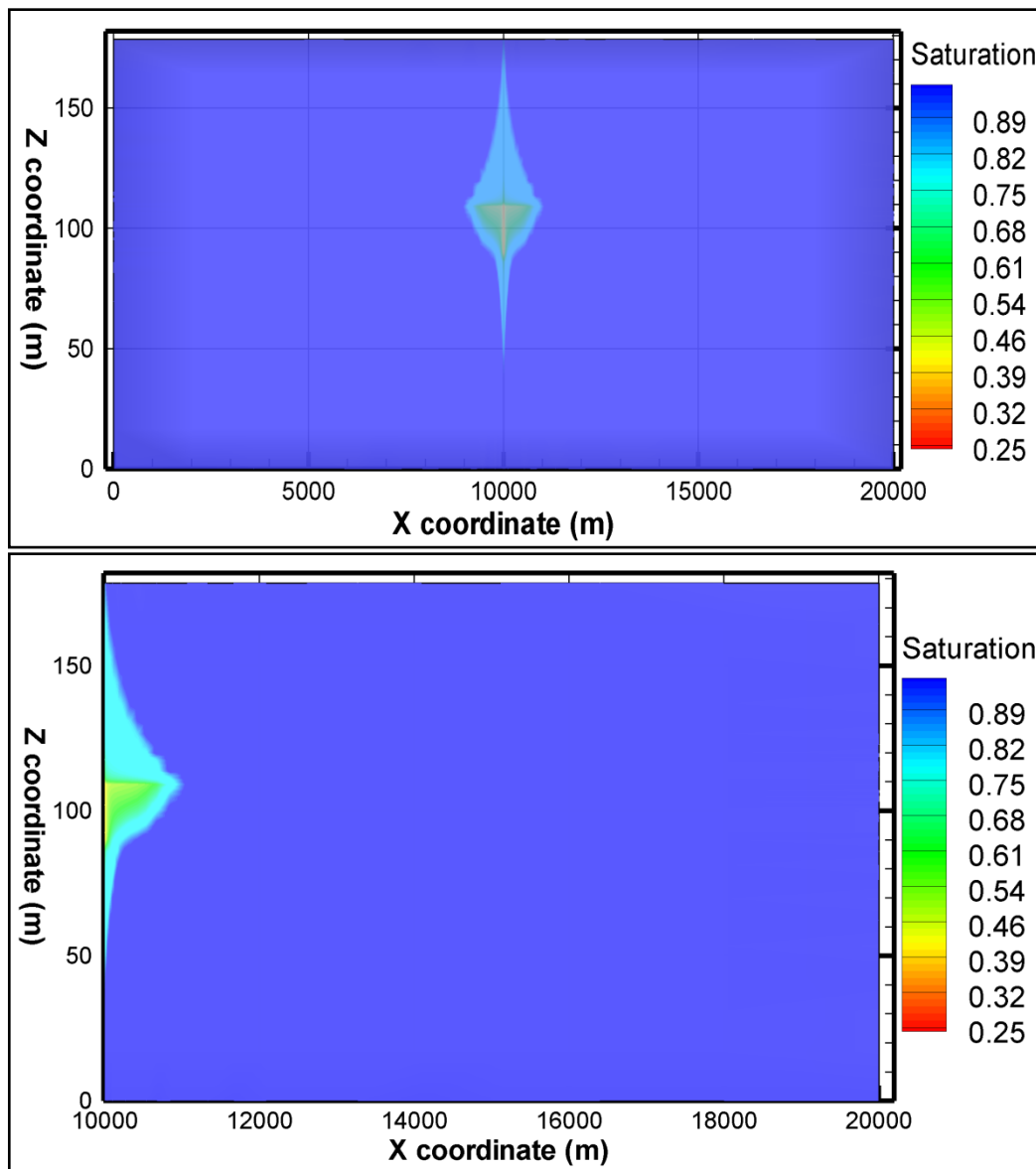
Figure B11: The simulated water saturations from the van Genuchten RLP 3D model. Permeability in the caprock and bottom bed is equal to 10^{-15} m^2.
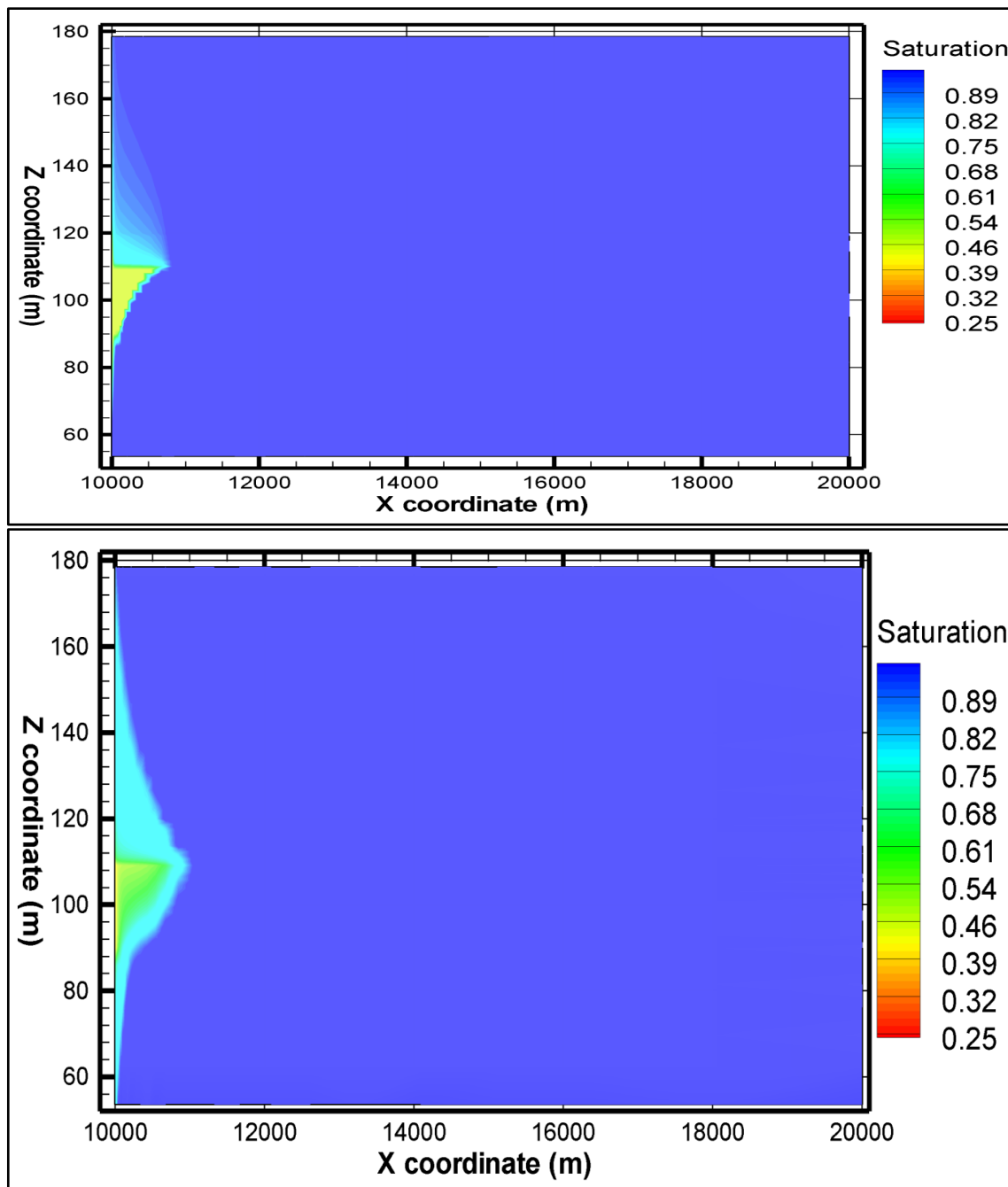
Figure B12: Comparison of the simulated water saturations of the linear RLP 3D model (upper) with the van Genuchten RLP 3D model (lower). Permeability in the caprock and bottom bed is equal to 10^{-15} m^2.
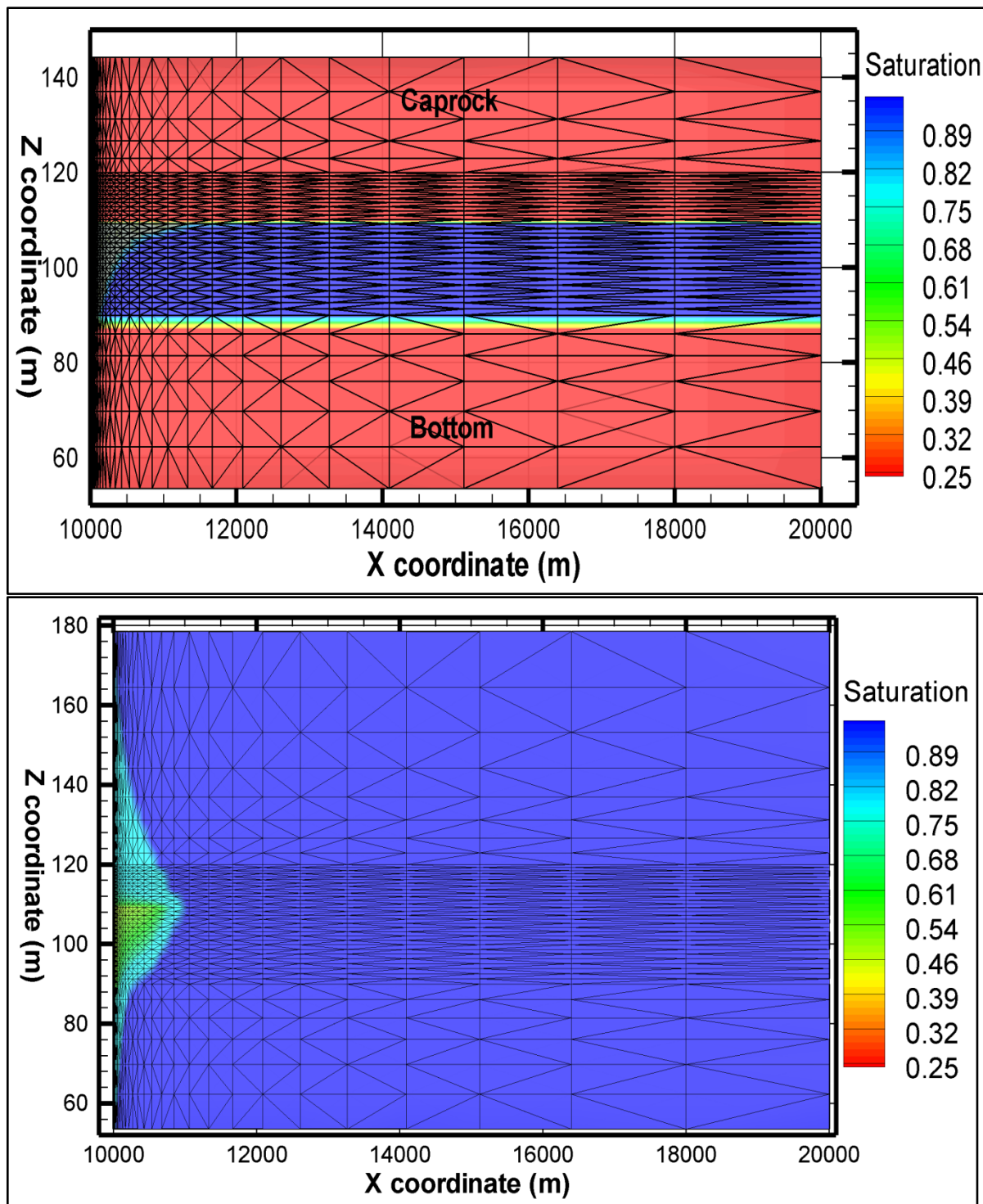
Figure B12: Comparison of the simulated water saturations of the linear RLP 3D model (upper, permeability in the caprock and bottom bed is equal to 10^{-19} m^2) with the van Genuchten RLP 3D model (lower, permeability in the caprock and bottom bed is equal to 10^{-15} m^2)
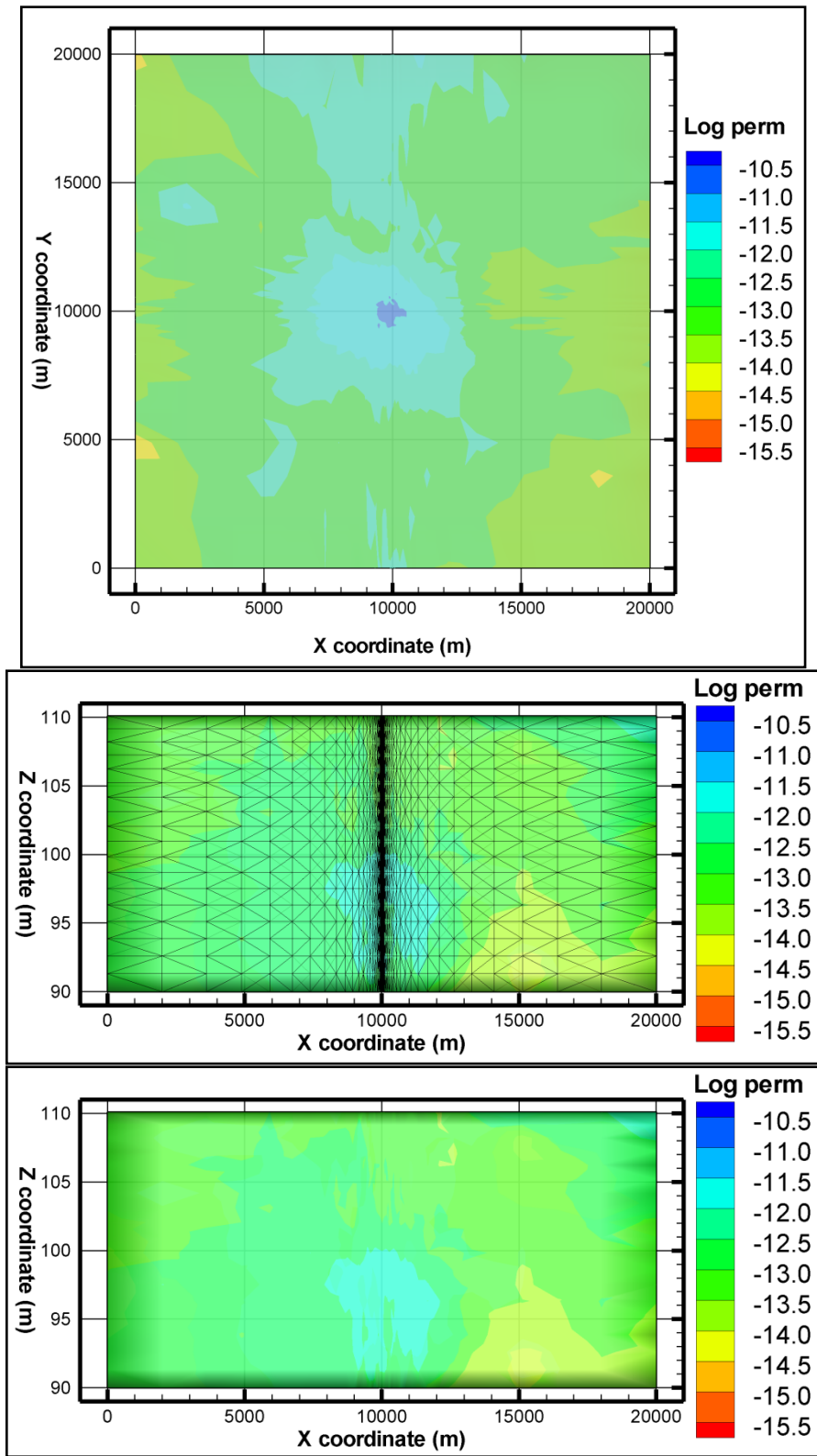
Figure B13: Heterogeneous permeability distribution in x-y (upper) and x-z (lower) plots
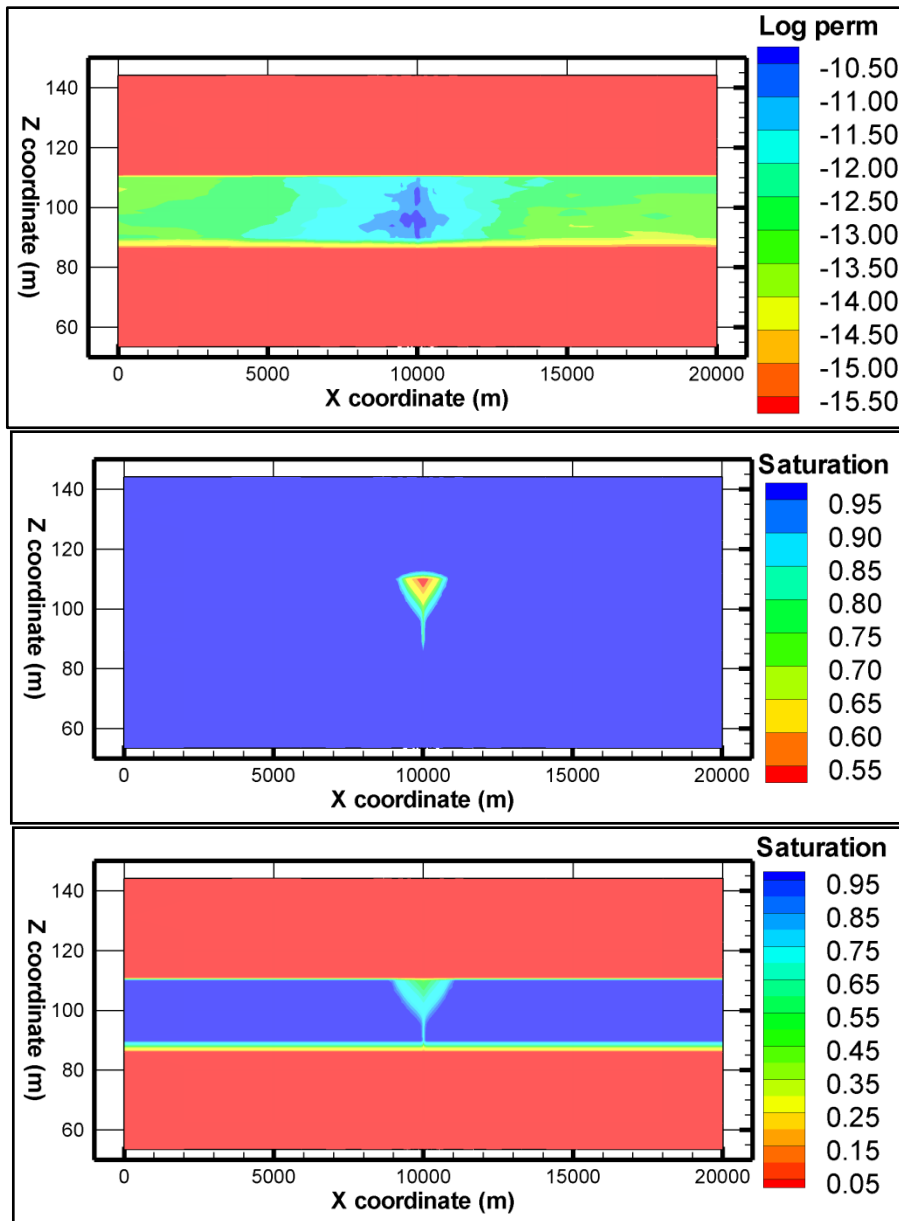
Figure B13: Heterogeneous permeability (upper) and water saturation (middle) and saturation excluding caprock (lower) in x-z plots

Appendix C: Validation of CO$_2$ Production : FEHM versus analytical solutions

Model verification for FEHM is first conducted for several cases with water only or CO$_2$ only, as analytical solutions for multiphase flow problems are not available.

A two-dimensional radial flow model is used, and the governing equation for the radial flow can be written as

$$\frac{\partial p}{\partial t} = \frac{k}{\phi \mu c_t} \frac{1}{r} \frac{\partial}{\partial r}\left(r \frac{\partial p}{\partial r}\right),$$
(C-1)

where p [Pa] is the pressure, k [m^2] is the permeability ϕ [-] is porosity, μ [Pa ·s] is the dynamic viscosity, c_t [Pa^{-1}] is the total compressibility, r [m] is the radial distance from the well, and t [s] is time.

The model configuration is shown in Figure C-1. The model domain has a radius of 20 km and a height of 100 m. The reservoir with a thickness of 60 m is confined by low permeable confining layers. A production well of wellbore radius r_w is located on the left. Various boundary conditions are specified in different cases described below.
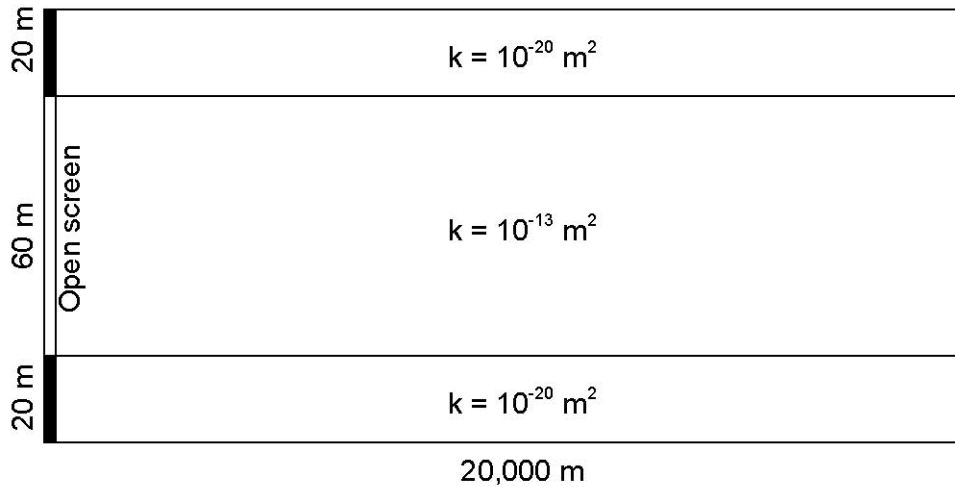

Figure C-1. Problem configuration for two-dimensional radial flow
Case 1. Water only; Infinity domain.
The initial and boundary conditions for the problem can be written as

$$p(r, t = 0) = p_0, \text{for } r > 0,$$
(4-2a)

$$\lim_{r \to 0}\left(r \frac{\partial p}{\partial r}\right) = -\frac{q_s B \mu}{2\pi k h},$$
(C-2b)

$$p(r \to \infty, t) = p_0, \text{for } t > 0,$$
(C-2c)

where p_0 [Pa] is the initial reservoir pressure, q_s [m^3/s] is the production rate, B [-] is the formation volume factor, and h [m] is the reservoir thickness. The solution can be expressed as

$$p(r,t) = p_0 + \frac{q_s B \mu}{4\pi k h} Ei\left(-\frac{\phi \mu c_t}{4k}\frac{r^2}{t}\right),$$

(C-3)

where $Ei(x) = \int_{-\infty}^{x} e^t t^{-1} dt$ is a standard mathematical function called the exponential integral. This function can be well approximated by $Ei(-x) = \ln(\gamma x)$, where $\gamma = e^{0.5772} = 1.781$ is related to the Euler constant 0.5772, if the following condition is satisfied:

$$\frac{\phi \mu c_t}{4k}\frac{r^2}{t} < 0.01,$$

(C-4)

and the solution (1-3) becomes

$$p(r,t) = p_0 - \frac{q_s B \mu}{4\pi k h}\left(\ln\frac{kt}{\phi \mu c_t r^2} + 0.80907\right).$$

(C-5)

For FEHM simulations, while the vertical resolution is 0.5 m, the horizontal grid size increases from about 0.01 m near the wellbore to about 1132 m at the right boundary.   The parameter values for this case are:

p_0 = 11 MPa
q_s = 1.21 × 10^{-4} m^3/s
B = 1.0 [-],
h = 60 m
k = 1. × 10^{-13} m^2
ϕ = 0.1
μ = 7.056 × 10^{-4} Pa ·s (at 36 °C)
c_t = 4.6 × 10^{-7} Pa^{-1}

Note that the total compressibility in the analytical solution is not a parameter in FEHM input. Instead, specific storage Ss (4.5 × 10^{-4} Pa^{-1}) is used, which can be converted to total compressibility by [Narasimhan and Kanehiro, 1980]: $c_t = S_s / \rho g \phi$, where ρ [kg/m^3] is the density of water, and g [m^2/s] is the gravitational constant. The comparison of pressure derived from the analytical solution and the FEHM numerical simulation along a radial profile z = 50 m (the central line in the middle of the reservoir) is illustrated in Figure C-2. It is seen that FEHM produces almost identical results as the analytical solution does. The figure also shows that the curves become straight lines on the semi-log plot, as indicated by equations (C-4) and (C-5).
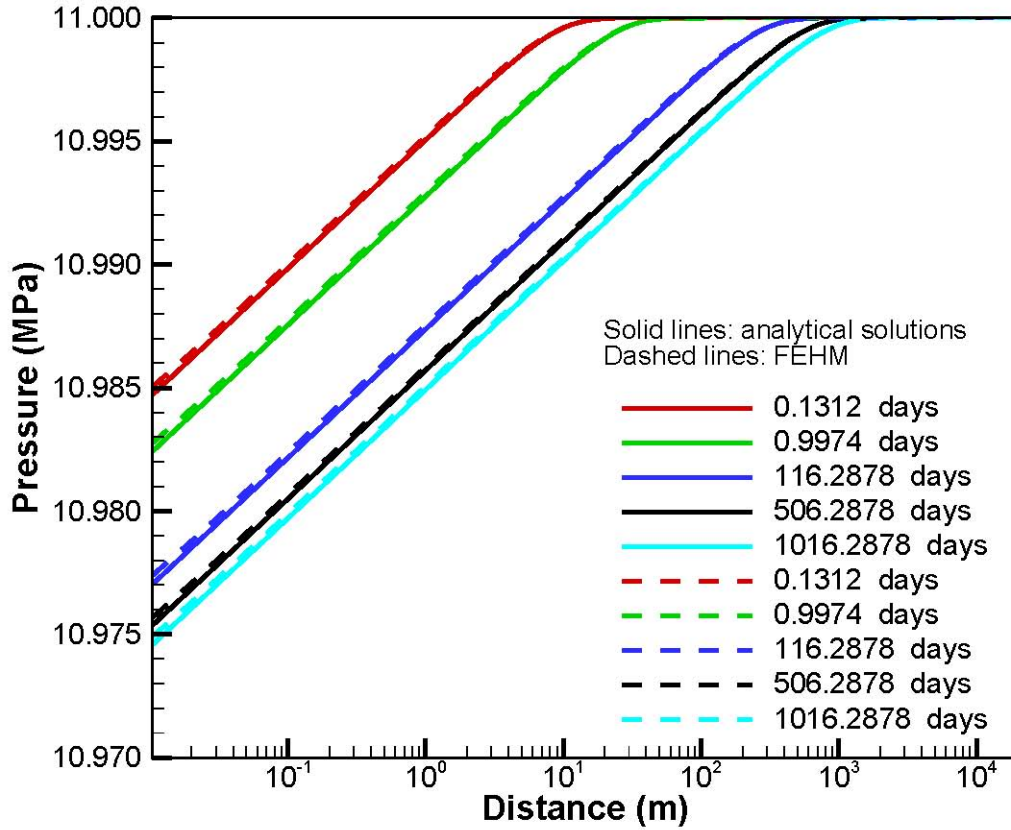
Figure C-2. Comparisons of water pressure profiles derived from analytical solutions and FEHM simulations for several selected times for initial and boundary conditions in Equations (1-2a)-(1-2c).

Case 2. Water only; Circular cylinder with fixed pressure at both borehole and external boundary
The initial and boundary conditions

$$p(r, t = 0) = p_0, \text{for } r > 0, \tag{C-6a}$$

$$p(r = r_w, t) = p_w, \tag{C-6b}$$

$$p(r = r_e, t) = p_0, \tag{C-6c}$$

where p_w [Pa] is the pressure at the well, r_w [m] is the wellbore radius, and r_e [m] is external radius of the drainage area. The solution can be derived:

$$p(r,t) = p_0 - (p_0 - p_w) \left[\frac{\ln(r_D/r_{eD})}{\ln(1/r_{eD})} - \pi \sum_{n=1}^{\infty} \frac{e^{-\alpha_n^2 t_D} J_0^2(\alpha_n r_{eD})}{J_0^2(\alpha_n) - J_0^2(\alpha_n r_{eD})} \left[J_0(\alpha_n) Y_0(\alpha_n r_D) - Y_0(\alpha_n) J_0(\alpha_n r_D) \right] \right] \tag{C-7}$$

where $r_D = r/r_w$, $r_{eD} = r_e/r_w$, and $t_D = kt/(\phi\mu c_t r_w^2)$ are dimensionless variables, J_0 and Y_0 are respectively the Bessel functions of order zero of the first and second kind, and the α_n are the positive roots of the following equation

$$J_0(\alpha)Y_0(\alpha r_{eD}) - Y_0(\alpha)J_0(\alpha r_{eD}) = 0 \qquad \text{(C-8)}$$

The solution in Equation (C-7) contains an infinite series that needs to be truncated. A numerical investigation indicates that the series converges after about 500 terms. In fact, the differences between solutions with 600, 700, 800, and 900 are indistinguishable with that of 1000 terms. To ensure the accuracy, we truncated the series with 1,000 terms (in accordingly, Equation C-8 needs to be solved for the first 1,000 positive roots). The analytical solutions at different times are illustrated in Figure C-3 (solid lines). The results from FEHM simulations (dashed lines) are compared against the analytical solutions. The comparison indicates that FEHM performs very well.
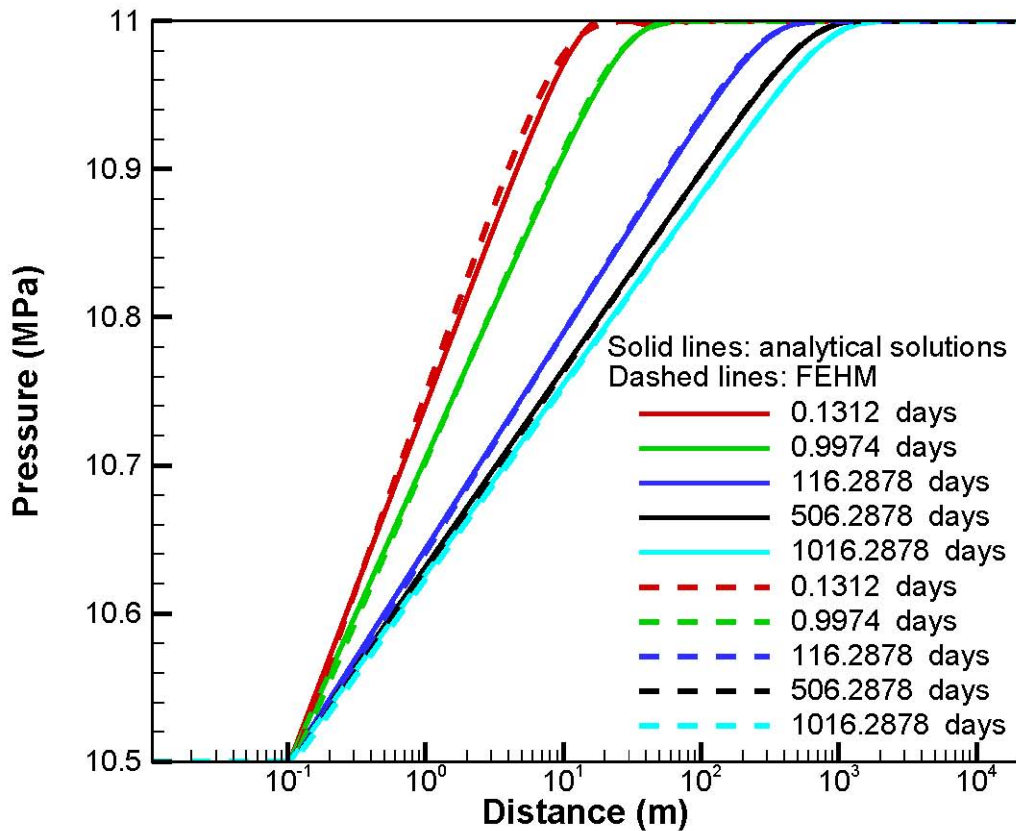

Figure C-3. Comparisons of water pressure profiles derived from analytical solutions and FEHM simulations for several selected times for initial and boundary conditions in Equations (C-6a)-(C-6c).

Case 3. CO_2 only; Circular cylinder with fixed pressure at both borehole and external boundary
This case is same as Case 2, except that the reservoir is saturated with CO_2 rather than water as in Case 2. Some parameter values used in FEHM are:

$p_0 = 11$ MPa
$p_w = 10.5$ MPa (at borehole)
$P_e = 11$ MPa (external boundary)
$B = 1.0$ [-],
$h = 60$ m
$k = 1. \times 10^{-13}$ m^2
$\phi = 0.15$
$\mu = 7.056 \times 10^{-4}$ Pa ·s (at 36 °C)
$c_t = 4.6 \times 10^{-7}$ Pa^{-1}
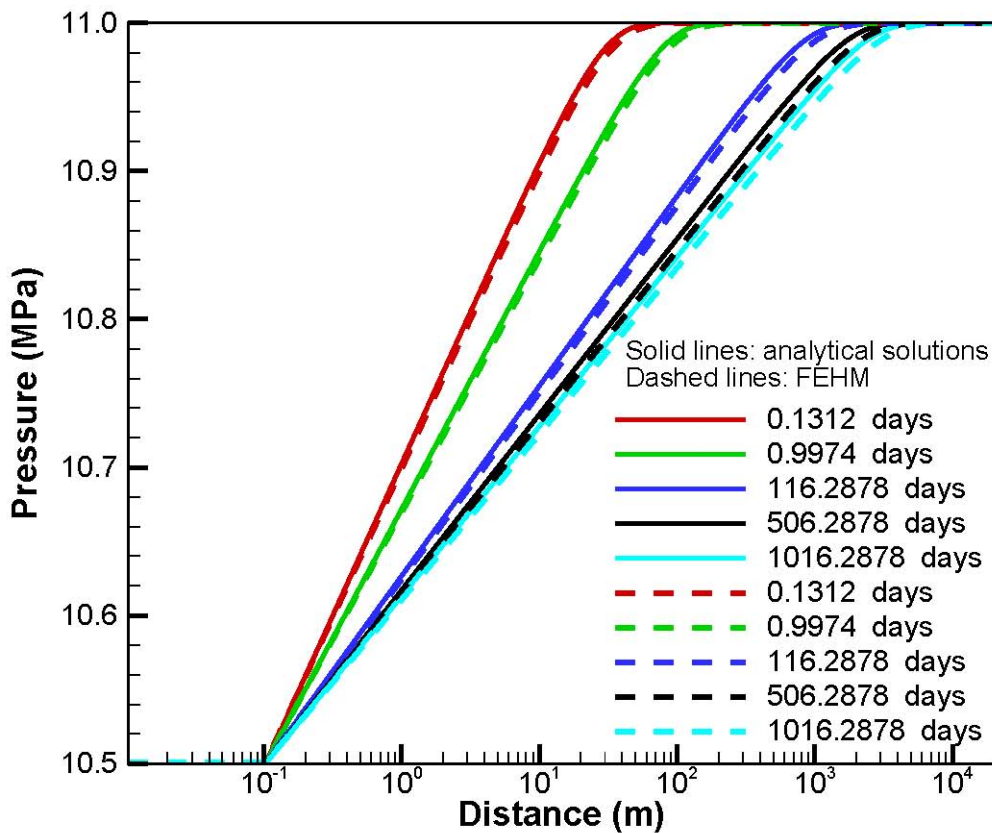$\rho = 733.05$ kg/ m^3 (at36 °C and pressure of 11 MPa)

Figure C-4. Comparisons of CO_2 pressure profiles derived from analytical solutions and FEHM simulations for several selected times for initial and boundary conditions in Equations (C-6a)-(C-6c).

Case 4. CO_2 only; Circular cylinder with fixed production rate at the borehole and fixed pressure at external boundary

The initial and boundary conditions

$$p(r, t = 0) = p_0, \text{for } r > 0, \tag{C-9a}$$

$$\left.\frac{\partial p}{\partial r}\right|_{r=r_w} = -\frac{q_s B \mu}{2\pi k h r_w}, \tag{C-9b}$$

$$p(r = r_e, t) = p_0, \tag{C-9c}$$

The solution can be derived:

$$p(r, t) = p_0 - \frac{q_s B \mu}{2\pi k h}\left[-\ln\left(\frac{r_D}{r_{eD}}\right) + \pi \sum_{n=1}^{\infty} \frac{e^{-\alpha_n^2 t_D} J_0^2(\alpha_n r_{eD})}{J_1^2(\alpha_n) - J_0^2(\alpha_n r_{eD})}\left[Y_1(\alpha_n) J_0(\alpha_n r_D) - J_1(\alpha_n) Y_0(\alpha_n r_D)\right]\right], \tag{C-10}$$

where $r_D = r/r_w$, $r_{eD} = r_e/r_w$, and $t_D = kt/(\phi \mu c_t r_w^2)$ are dimensionless variables, J_0 and Y_0 are respectively the Bessel functions of order zero of the first and second kind, J_1 and Y_1 are respectively the Bessel functions of first order of the first and second kind, and the α_n are the positive roots of the following equation

$$J_1(\alpha) Y_0(\alpha r_{eD}) - Y_1(\alpha) J_0(\alpha r_{eD}) = 0. \tag{C-11}$$

The analytical solution of the pressure at the production well as a function of time is compared against the FEHM results Figure C-5..
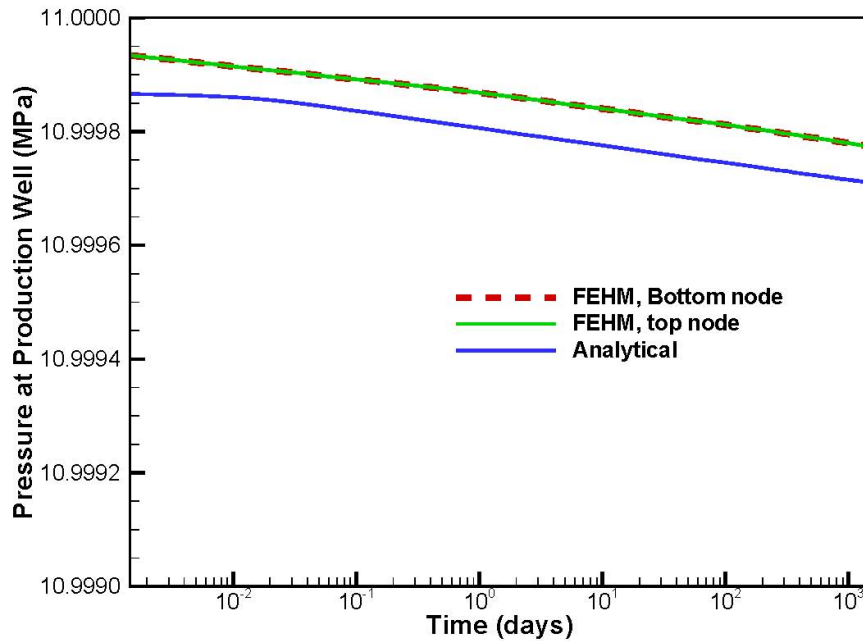

Figure C-5. Comparisons of CO_2 pressure profiles derived from the analytical solution, Equation (C-10), and FEHM simulations for several selected times for initial and boundary conditions in Equations (C-9a)-(C-9c).

Finally, we present comparison between the analytical solution and FEHM for two examples where drawdown is more significant. Figure C-6 shows results for Case 1 (thick) while figure C-7 shows results for Case 2 (thin). In both cases, the solutions are nearly exact to well past 100 days. The divergence at late time is expected, as FEHM has a continuously varying compressibility while the analytical solution uses a single value for the full range of pressures.
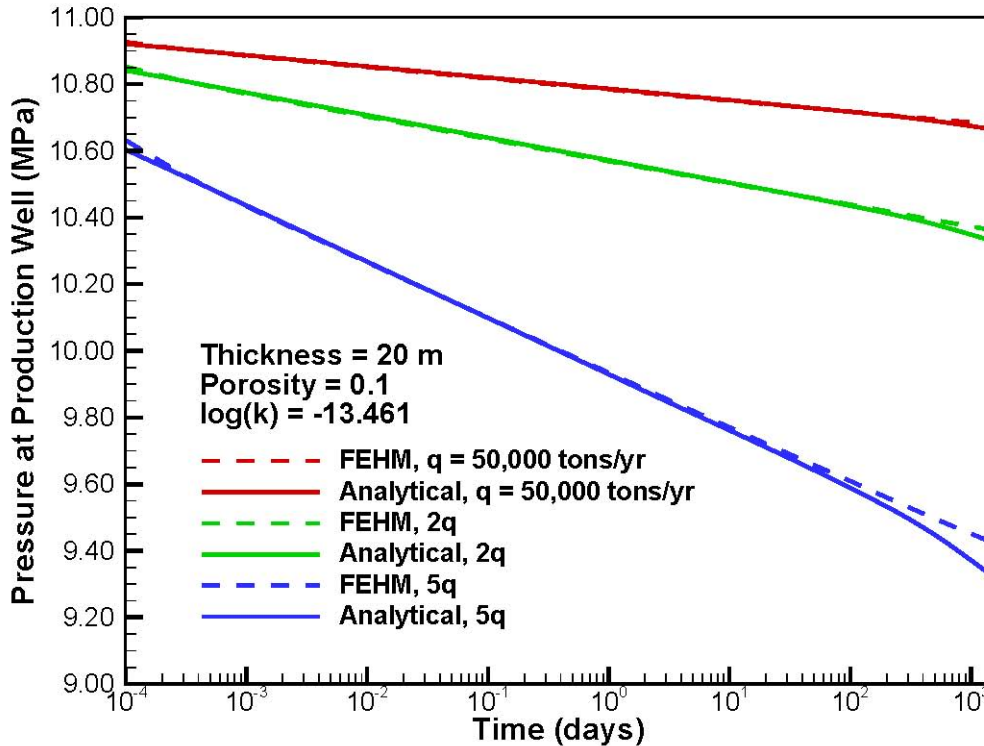

Figure C-6. Comparisons of CO_2 pressure profiles derived from the analytical solution, Equation (C-10), and FEHM simulations for several selected times for flow rates from 0.05 to 0.25 MT/yr for Case 1, a thick, lower permeability reservoir.
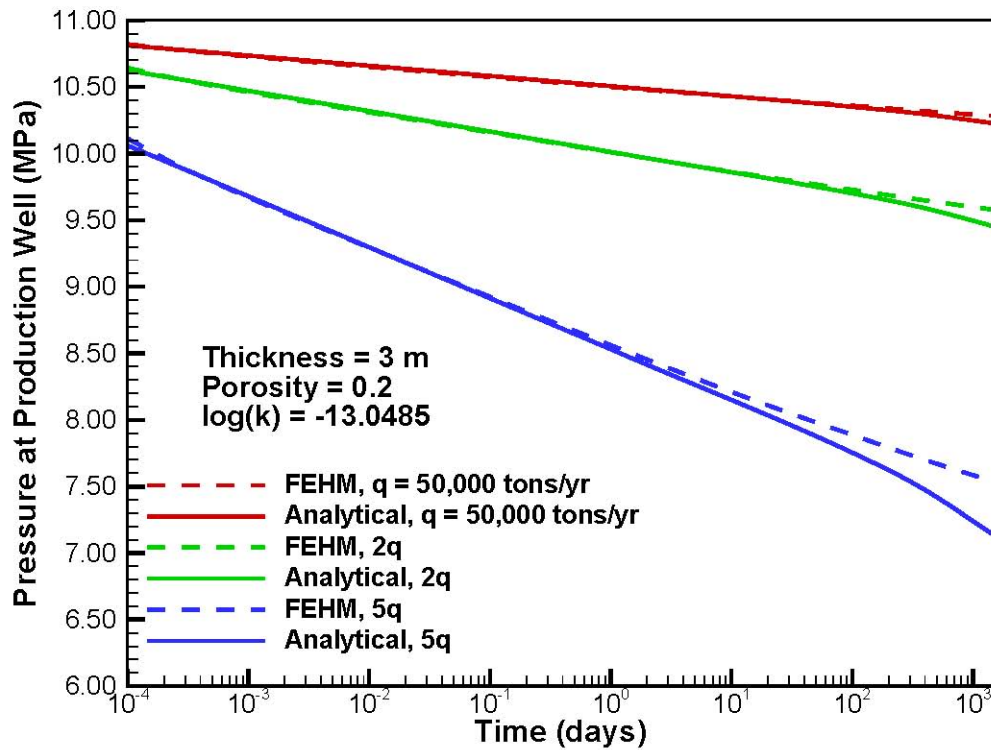
Figure C-7. Comparisons of CO_2 pressure profiles derived from the analytical solution, Equation (C-10), and FEHM simulations for several selected times for flow rates from 0.05 to 0.25 MT/yr for Case 2, a thin, higher permeability reservoir.